Basal ppGpp signalling by SpoT integrates metabolism with acid resistance

Yueyue Liu[1#], Muriel Leandra Schicketanz[1#^], Xichuan Zhai[2], Ling Deng[2], Kenn Gerdes[3], Yong Everett Zhang[1*]

[1] Department of Biology, University of Copenhagen, DK-2200 Copenhagen, Denmark

[2] Section of Food Microbiology, Gut Health, and Fermentation, Department of Food Science, University of Copenhagen, Rolighedsvej 26, 1958 Frederiksberg C, Denmark

[3] Independent Researcher, Copenhagen, Denmark

[#] Y.Y.L. and M.L.S. contributed equally to this work.

^ Current address: Novonesis A/S, Kgs. Lyngby, Denmark

*Correspondence: Yong Everett Zhang zhangy830328@gmail.com

Running title: Basal ppGpp integrates metabolism and acid resistance

Abstract

Bacteria maintain low basal levels of the alarmone ppGpp during steady-state growth, yet how this basal state is established and why it matters physiologically remain poorly understood. Here, we show that basal ppGpp represents an actively maintained regulatory state that coordinates metabolic homeostasis with stress resistance. Using a targeted perturbation of SpoT regulation in *Escherichia coli*, we uncover a sharp requirement for a sub-basal yet non-zero ppGpp pool to sustain growth in minimal medium and survival under extreme acid stress. Disruption of this basal state leads to misallocation of metabolic flux into arginine biosynthesis, depletion of glutamate, and collapse of the glutamate-dependent Gad acid resistance system. Through intragenic suppressor analysis, enzymatic perturbations, and protein-level feedback measurements, we further demonstrate that SpoT intrinsically tunes basal ppGpp through a distributed intramolecular regulatory network coupled to negative feedback control of SpoT abundance. This regulatory logic stabilizes ppGpp within a narrow physiological window, below the threshold of canonical stringent response activation. The requirement for SpoT-dependent basal ppGpp regulation is conserved in pathogenic *Salmonella* and *Shigella*. Together, our findings establish basal ppGpp as a distinct and actively regulated signaling regime that integrates metabolism and stress preparedness beyond acute starvation responses.

KEYWORDS: basal ppGpp, SpoT, stringent response, metabolic homeostasis, acid resistance, Gad system

Introduction

Bacteria inhabit environments that fluctuate rapidly and often impose multiple, simultaneous stresses. Successful survival under such conditions requires tight coordination between core metabolic processes and stress-protective responses in a manner that preserves essential resources while maintaining viability. For enteric bacteria in particular, the ability to balance nutrient availability with resistance to extreme acidity - such as that encountered during gastric passage - is a key determinant of ecological fitness and pathogenic potential[1,2]. Despite extensive study of individual stress-response pathways, how bacteria integrate metabolic homeostasis with acid resistance remains incompletely understood.

A central regulator of bacterial metabolic adaptation is the stringent response, a conserved signaling network mediated by the alarmone guanosine tetra- and pentaphosphate (ppGpp)[3-6]. Canonically, ppGpp is produced in large bursts upon amino acid starvation, when uncharged tRNAs activate the ribosome-associated enzyme RelA in *Escherichia coli*[7-11]. This acute increase in ppGpp rapidly remodels transcription, repressing stable RNA synthesis while redirecting metabolic flux toward amino acid biosynthesis[12-16]. In parallel, ppGpp directly targets numerous metabolic enzymes, rebalancing nucleotide and amino acid pools[17-21]. This RelA-driven stringent response has therefore been widely viewed as an emergency program that facilitates rapid bacterial adaptation to acute nutrient stress.

Once this acute response has restored metabolic balance and growth resumes, ppGpp levels decline but do not return to zero. In contrast to the well-characterized high-amplitude stringent response, much less is known about the physiological role of these low, basal levels of ppGpp that persist during adapted growth[22]. Basal ppGpp is believed to be primarily controlled by SpoT, a bifunctional enzyme that both synthesizes and hydrolyzes ppGpp[23] and responds to diverse

58 environmental cues distinct from amino acid starvation[24-30]. Genetic and physiological studies have
59 established that SpoT activity is essential for viability, virulence, and stress adaptation across many
60 bacterial species[3,31,32]. However, because SpoT's hydrolase activity is required to counterbalance
61 RelA-mediated ppGpp synthesis, direct analysis of SpoT regulatory function has been challenging.
62 As a result, basal ppGpp has often been treated as a passive background signal rather than an active
63 regulatory regime with distinct physiological roles.

64 Acid resistance provides a compelling context in which to examine basal ppGpp regulation. *E. coli*
65 is capable of surviving exposure to pH values as low as 2.5 through multiple acid resistance
66 systems, among which the glutamate-dependent Gad system is the most effective[2,33,34]. This system
67 uses cytoplasmic glutamate decarboxylases (GadA and GadB) to convert glutamate to γ-
68 aminobutyrate, consuming intracellular protons, while the GadC antiporter exchanges γ-
69 aminobutyrate for extracellular glutamate to sustain the cycle[35,36]. The Gad system is subject to
70 complex regulation involving transcriptional activators (GadE), global stress regulators (e.g.,
71 ppGpp), and growth-phase signals (e.g., RpoS)[2,36]. Notably, glutamate itself occupies a central
72 position in cellular metabolism, serving as a key nitrogen donor and metabolic hub. How bacteria
73 coordinate glutamate homeostasis with glutamate-dependent acid resistance under nutrient-limited
74 conditions remains poorly understood.

75 Here, we set out to investigate how SpoT-dependent basal ppGpp signaling contributes to the
76 integration of amino acid metabolism with acid resistance during nutrient-limited growth. As an
77 entry point into this poorly understood regulatory regime, we focused on a strictly conserved
78 histidine residue (H414) within the C-terminal regulatory region of SpoT. Perturbation of this
79 residue resulted in pronounced physiological imbalances, including altered metabolic flux through
80 arginine biosynthesis, depletion of intracellular glutamate, and reduced expression of the glutamate-

81 dependent Gad acid resistance system. These observations provided a framework for systematically
82 dissecting how SpoT-dependent basal ppGpp supports metabolic and stress-response homeostasis.

83 Because SpoT homologs are conserved across enteric bacteria, we further asked whether the
84 regulatory principles revealed by this approach extend beyond *E. coli*. Addressing this question
85 allowed us to evaluate whether SpoT-dependent basal ppGpp represents a species-specific
86 phenomenon or a more general regulatory regime. In this context, our study seeks to expand the
87 functional scope of ppGpp signaling beyond RelA-mediated acute starvation responses to include a
88 role in coordinating metabolism and stress resistance during nutrient-limited growth.

89 **Results**

90 **Perturbation of SpoT regulation leads to severe growth defects in minimal medium**

91 To examine how SpoT-dependent regulation supports growth under nutrient-limited conditions
92 independently of RelA, we focused on the conserved C-terminal regulatory region of SpoT, which
93 is highly conserved among RelA/SpoT homologs but remains poorly understood mechanistically.
94 Sequence alignment identified a strictly conserved histidine residue (H414 in *E. coli* SpoT) within
95 the TGS domain, corresponding to H432 in RelA (**Extended Data Fig. 1a, 1b**), a residue cucial for
96 sensing amino acid starvation[8-11].

97 As a genetic probe of this conserved regulatory region, we generated a SpoT H414A substitution in
98 a *ΔrelA* background. While the Δ*relA spoT*^{wt} (hereafter referred to as *spoT*^{wt}) strain grew normally,
99 the H414A mutant (*spoT*^{H414A}) displayed a severe and unexpected growth defect on glucose
100 minimal medium (M9Glc), both on solid and in liquid culture (**Fig. 1a, 1b**). This unanticipated
101 phenotype indicated that SpoT H414 plays a critical role in supporting growth under nutrient-
102 limited conditions and prompted further investigation into its underlying molecular basis.

103 **Loss of SpoT regulation disrupts transcriptional programs for stress and acid resistance**

104 To gain insight into the molecular defects underlying the growth failure of *spoT*^{H414A} cells, we
105 performed transcriptomic analysis of the *spoT*^{H414A} and *spoT*^{wt} strains. Because *spoT*^{H414A} cells
106 failed to proliferate in M9Glc, cultures were incubated under identical conditions until the *spoT*^{wt}
107 strain entered early exponential phase, at which point RNA was harvested from both strains
108 (**Extended Data Fig. 1c**).

109 This analysis revealed extensive transcriptional dysregulation in *spoT*^{H414A} cells, with strong
110 repression of stress adaptation and acid resistance genes. Among the most prominently
111 downregulated loci were the glutamate-dependent Gad acid resistance system (*gadE*, *gadX*, *gadW*,
112 *gadA*, *gadB*, *gadC*), as well as additional components of the acid fitness island, including the
113 periplasmic chaperones *hdeAB* (**Fig. 2a, 2b**). Genes associated with osmotic and general stress
114 responses were similarly reduced; in contrast, genes linked to phage shock and SOS responses were
115 strongly induced (**Extended Data Fig. 1d-f**), indicating a broad physiological imbalance**.** The
116 pronounced repression of acid resistance pathways indicated a defect in acid survival and prompted
117 direct physiological testing of *spoT*^{H414A} cells under acidic conditions.

118 **SpoT, but not RelA, is required for survival under extreme acid stress**

119 Guided by the pronounced transcriptional repression of acid resistance genes in *spoT*^{H414A} cells, we
120 next examined survival under lethal acid stress. Upon exposure to pH2.5, *spoT*^{H414A} cells exhibited
121 profound acid sensitivity, with viability declining rapidly and no detectable survivors after 60
122 minutes (**Fig. 2c**). In contrast, both the parental wild-type strain and the *spoT*^{wt} strain survived acid
123 challenge efficiently, indicating that RelA is dispensable for acid resistance under this condition.

124 Notably, despite the severe acid sensitivity of *spoT*^{H414A} cells, viability under neutral, well-buffered
125 conditions (M9Glc) was preserved (**Extended Data Fig. 1g**), suggesting that SpoT H414 is
126 specifically required to support stress preparedness rather than basal cell viability. Together, these
127 results identify SpoT, rather than RelA, is required to support survival under extreme acid stress in
128 *E. coli*.

129 **Loss of SpoT regulation drives arginine overflow and glutamate depletion**

130 To define the metabolic basis of the growth defect observed in *spoT*^{H414A} cells, we examined
131 transcriptomic changes in central metabolic pathways. While expression of many amino acid
132 biosynthetic genes was modestly reduced, one pathway was prominently induced: arginine
133 biosynthesis was strongly and coordinately upregulated (**Fig. 3a, 3b**). All the nine enzymes of the
134 arginine biosynthetic pathway exhibited significantly increased expression, together with *carAB*,
135 which supplies carbamoylphosphate to this pathway. This pattern indicates a pronounced
136 redirection of metabolic flux toward arginine production.

137 In contrast, genes directing carbamoylphosphate toward pyrimidine nucleotide biosynthesis were
138 downregulated, suggesting selective diversion of this shared intermediate rather than a generalized
139 increase in anabolic metabolism. Because arginine biosynthesis consumes glutamate as a precursor,
140 the coordinated induction of the *arg* operons is predicted to substantially deplete intracellular
141 glutamate pools**.**

142 In parallel with arginine pathway induction, genes involved in *de novo* purine nucleotide
143 biosynthesis were broadly upregulated (**Extended Data Fig. 2**). Many of these reactions consume
144 glutamine as a nitrogen donor, which is regenerated from glutamate, thereby imposing an
145 additional, indirect demand on glutamate availability. Thus, the combined activation of arginine and

146 purine biosynthetic programs is expected to exacerbate glutamate depletion, compounding the
147 metabolic imbalance caused by SpoT H414A mutation.

148 Together, these transcriptional signatures point to a misallocation of metabolic resources upon loss
149 of SpoT H414, with excessive flux into arginine biosynthesis and increased purine nucleotide
150 production collectively depleting glutamate. Given the central role of glutamate in both metabolism
151 and acid resistance, this imbalance offers a unifying explanation for the growth and stress survival
152 defects observed in *spoT*^{H414A} cells and motivated direct tests of glutamate availability in subsequent
153 experiments.

154 **Glutamate depletion contributes to growth defects caused by SpoT perturbation**

155 Prompted by the transcriptomic evidence for glutamate depletion, we tested whether exogenous
156 supplementation could restore growth. Addition of glutamate to M9Glc robustly improved growth
157 of *spoT*^{H414A} cells, substantially shortening the lag phase and increasing final biomass (**Fig. 3c**). In
158 contrast, supplementation with arginine or uracil failed to restore growth, and co-supplementation
159 with glutamate conferred no additional benefit.

160 Among all 20 amino acids, supplementation with glutamine, asparagine, or proline partially
161 restored growth, consistent with their metabolic proximity to glutamate, but none matched the effect
162 of glutamate itself (**Extended Data Fig. 3a**). Increasing the concentration of glutamate up to
163 tenfold failed to further improve growth (**Extended Data Fig. 3b**), and combining glutamate with
164 glutamine, asparagine, or proline did not enhance regrowth beyond that achieved with glutamate
165 alone (**Extended Data Fig. 3c**). In contrast, supplementation with all 20 amino acids fully restored
166 the growth defect of *spoT*^{H414A} cells to a level exceeding that of the *spoT*^{wt} strain (**Extended Data**
167 **Fig. 3d**), indicating that glutamate depletion represents a dominant, though not exclusive, metabolic

168 limitation associated with SpoT H414A dysfunction. Importantly, glutamate supplementation had
169 only minimal effects on the growth of a ppGpp^0 (*ΔrelA ΔspoT*) strain (**Extended Data Fig. 3e**),
170 indicating that growth rescue requires SpoT-dependent basal ppGpp rather than nonspecific
171 nutritional supplementation.

172 To directly test whether arginine biosynthesis drives glutamate depletion, we deleted *argA*,
173 encoding the first committed enzyme of the arginine biosynthetic pathway. As expected, the
174 resulting *spoT*^{wt} *ΔargA* strain failed to grow in M9Glc; this defect was fully rescued by arginine
175 supplementation but not by glutamate, confirming that growth limitation in this background reflects
176 arginine auxotrophy rather than glutamate deficiency (**Fig. 3d**). Similarly, the *spoT*^{H414A} *ΔargA*
177 strain failed to grow in M9Glc (**Fig. 3d**). Notably, arginine, but not glutamate, largely restored
178 growth in this background, indicating that blocking arginine biosynthesis prevents excessive
179 glutamate consumption and alleviates the growth defect of *spoT*^{H414A}.

180 Arginine biosynthesis is normally subject to feedback inhibition through ArgA. Conversely, we
181 found that artificial overexpression of a feedback-resistant ArgA variant (ArgA^{H15Y})[37] via IPTG
182 induction phenocopied the *spoT*^{H414A} growth defect in M9Glc, and this delayed growth was
183 substantially alleviated by glutamate supplementation (**Fig. 3e**). Together, these results establish
184 that SpoT H414 restrains arginine-driven glutamate consumption, thereby preserving amino acid
185 homeostasis required for growth in minimal medium.

186 **SpoT perturbation compromises glutamate-dependent acid resistance**

187 Because glutamate is the essential substrate for the Gad acid resistance system, we next asked
188 whether glutamate depletion contributes to the acid sensitivity of *spoT*^{H414A} cells. Supplementation
189 of the acid challenge medium with glutamate fully rescued survival during short-term acid exposure

190 and markedly improved long-term viability (**Fig. 4a**). In contrast, supplementation with arginine or
191 lysine provided only modest protection (**Extended Data Fig. 4a**), consistent with the prominent
192 contribution of the glutamate-dependent Gad system under extreme acid stress.

193 To determine whether impaired regulation of the Gad system accounted for the acid resistance
194 defect, we ectopically expressed *gadE*, the master transcriptional activator of Gad genes. Even low-
195 level expression of *gadE* significantly restored acid resistance in $spoT^{H414A}$ cells, and combined
196 supplementation with glutamate further enhanced survival (**Extended Data Fig 4b**). These
197 interventions did not alter acid resistance in $spoT^{wt}$ cells, indicating that the defect arises
198 specifically from SpoT dysfunction. Notably, despite its ability to restore acid survival, ectopic
199 expression of *gadE* failed to improve the growth of $spoT^{H414A}$ cells in M9Glc (**Extended Data Fig.**
200 **4c**). This functional separation indicates that impaired acid resistance is not sufficient to account for
201 the growth defect, which is more closely associated with glutamate depletion and broader metabolic
202 misallocation.

203 We further examined acid tolerance across a range of pH values. In addition to catastrophic
204 sensitivity at pH 2.5, $spoT^{H414A}$ cells exhibited reduced survival under mildly acidic conditions (pH
205 4.0-6.0) (**Fig. 4b, Extended Data Fig 4d**), consistent with a broader impairment of multiple acid
206 stress response pathways (**Extended Data Fig 4e**). Notably, these defects occurred despite
207 preserved viability under neutral pH conditions (**Extended Data Fig 1g**), indicating that SpoT-
208 mediated basal regulation selectively primes cells for acid stress rather than broadly supporting
209 growth.

210 **Intragenic suppression reveals intrinsic regulation within SpoT**

211 These findings raised a fundamental question of how SpoT activity is regulated to maintain the
212 physiological state underlying growth and stress resistance. The severe growth and acid resistance
213 defects of *spoT*^{H414A} cells suggested that H414 plays a central regulatory role in SpoT function. To
214 determine whether this phenotype reflected impaired regulation by trans-acting protein factors, we
215 first tested overexpression of established SpoT regulators, including ObgE[38], Rsd[39], YtfK[40], and
216 AcpP[25], none of which measurably restored growth of *spoT*^{H414A} cells in minimal medium
217 (**Extended Data Fig 5**). We further explored the possibility that H414 mediates regulation through
218 interaction with previously unidentified protein partners by introducing a photo-crosslinkable
219 unnatural amino acid at position 414 and performing UV-activated crosslinking under the same
220 growth conditions. Despite robust expression of full-length SpoT proteins, we did not detect
221 reproducible interactions with additional protein factors (**Extended Data Fig. 6**). Together, these
222 results suggested that the regulatory function of H414 is unlikely to be mediated by trans-acting
223 protein partners. We therefore pursued an unbiased genetic approach and isolated spontaneous
224 suppressor mutants capable of restoring growth of *spoT*^{H414A} cells on M9Glc. After prolonged
225 incubation (24-72 h), colonies of varying sizes emerged on M9Glc agar (**Fig. 5a**).

226 Analysis of 50 independently isolated suppressors revealed that the strongest suppressors
227 predominantly carried secondary mutations within the *spoT* gene itself. Among large-colony
228 suppressors, we identified recurrent substitutions at residues G334 (G334S; supA, 17/50), E364
229 (E364K; supB, 5/50), and S463 (S463R; sup41, 9/50) as well as a small in-frame deletion within
230 the synthetase domain (ΔV_{200}IKE; sup17, 3/50) (**Fig. 5b**). Whole-genome sequencing of small-
231 colony suppressors lacking *spoT* mutations identified a single mutation in *rpoB* (K1262Q), which is
232 likely similar as the previously described stringent-response suppressors[41] supporting the growth of
233 ppGpp^0 strain on minimal media, and therefore these strains were excluded from further analysis.

234 Reconstruction of the identified *spoT* suppressor mutations in a clean background fully
235 recapitulated growth restoration of *spoT*^{H414A} in M9Glc (**Extended Data Fig 7**), whereas deletion of
236 *spoT* in the suppressor strains abolished growth (**Fig. 5c**). These results demonstrate that intragenic
237 mutations within SpoT are both necessary and sufficient to suppress the *spoT*^{H414A} growth defect.

238 We next asked whether suppression of the growth defect was accompanied by restoration of acid
239 resistance. All four *spoT* suppressor strains exhibited improved survival under lethal acid challenge
240 (pH 2.5) compared to the parental *spoT*^{H414A} strain, although the degree of rescue varied (**Fig. 5d**).
241 The suppressor sup41 displayed the most robust acid resistance, followed by supB, supA and sup17.
242 Supplementation of the acid challenge medium with glutamate further enhanced survival across all
243 suppressor strains, with particularly pronounced effects in the weaker suppressors supB and sup17
244 (**Fig. 5d**). These differences suggest that individual suppressor mutations restore SpoT function
245 through distinct mechanisms that differentially affect glutamate homeostasis and stress
246 preparedness.

247 Together, these results show that intragenic suppression of SpoT H414A simultaneously restores
248 growth and acid resistance, reinforcing the link between SpoT activity, metabolic balance, and
249 stress survival.

250 **Basal ppGpp is actively maintained within a narrow functional window**

251 Given SpoT's dual role as a ppGpp synthase and hydrolase, we next asked whether the growth
252 defect of *spoT*^{H414A} cells is associated with altered ppGpp homeostasis, and whether suppressor
253 mutations restore a physiologically relevant ppGpp state. To address this, we measured intracellular
254 ppGpp levels using ^{32}P-orthophosphate labeling and thin-layer chromatography[18]. As expected,
255 *spoT*^{wt} cells produced a readily detectable basal ppGpp signal, whereas *spoT*^{H414A} cells accumulated

256 only marginal, near-background levels of ppGpp (**Fig. 6a**). Notably, ppGpp levels in the suppressor
257 strains remained close to the detection limit and were not substantially elevated relative to *spoT*^{H414A}
258 cells.

259 This observation raised the possibility that either very small increases in ppGpp are sufficient to
260 restore physiological function, or that ppGpp turnover is highly dynamic in suppressor strains. To
261 distinguish between these possibilities, we genetically perturbed SpoT enzymatic activities.
262 Inactivation of the ppGpp synthetase activity of SpoT by the E319Q substitution in suppressor
263 backgrounds severely delayed or abolished growth recovery in M9Glc (**Fig. 6b**), demonstrating that
264 ppGpp synthesis is required for suppression. Conversely, inactivation of SpoT's hydrolase activity
265 by the H72A/D73A substitution led to robust ppGpp accumulation (**Fig. 6c**) and accelerated growth
266 resumption (**Fig. 6d**), indicating that suppressor strains produce ppGpp that is rapidly turned over
267 under basal conditions. Notably, the hydrolase-inactive variants of supA and sup17 could not be
268 obtained, likely due to the toxicity associated with excessive ppGpp accumulation.

269 Because C-terminal domains of RelA/SpoT homologs are known to regulate the catalytic activities
270 of the N-terminal enzymatic domains, we next systematically truncated these regulatory regions to
271 assess how suppressor mutations alter intramolecular control of SpoT activity. Consistent with this
272 model, truncation of individual C-terminal domains revealed that distinct suppressor mutations
273 differentially modify the contribution of these domains to growth control (**Extended Data Fig. 8**),
274 without abolishing the requirement for basal ppGpp synthesis. These findings indicate that SpoT
275 H414 functions within a broader intramolecular regulatory network that fine-tunes basal ppGpp
276 production, rather than acting as an isolated molecular switch.

277 Together, these data demonstrate that a sub-basal but non-zero ppGpp pool - close to the detection
278 limit of conventional assays - is sufficient to support growth in minimal medium, and that SpoT
279 activity is finely tuned to maintain this pool within a narrow physiological range.

280 **Negative feedback between ppGpp and SpoT abundance stabilizes basal ppGpp**

281 To investigate how SpoT activity is regulated, we examined SpoT protein levels using an antiserum
282 raised against the C-terminal regulatory domains of SpoT. Immunoblot analysis revealed that SpoT
283 protein levels were markedly elevated in *spoT*^{H414A} cells compared to *spoT*^{wt} and suppressor strains
284 (**Fig. 6e**).

285 Because *spoT*^{H414A} cells produce sub-basal ppGpp levels, whereas suppressor strains restore
286 physiological function with slightly elevated but tightly controlled ppGpp, these results suggest the
287 existence of a negative feedback mechanism in which basal ppGpp limits SpoT abundance. Such
288 feedback would stabilize intracellular ppGpp levels by adjusting SpoT protein concentration in
289 response to alarmone availability. This regulatory relationship provides a parsimonious mechanistic
290 framework for how SpoT may maintain a narrow basal ppGpp range sufficient for metabolic
291 homeostasis without eliciting an acute stringent response.

292 **Graded restoration of transcriptional programs reflects quantitative tuning of basal SpoT**
293 **activity**

294 To understand how suppressor mutations restore growth and acid resistance, we performed RNA
295 sequencing on the four suppressor strains. Parallel coordinates and multidimensional scaling
296 analyses revealed that strong suppressors (supA and sup41) clustered closely with *spoT*^{wt} cells,
297 whereas weaker suppressors (supB and sup17) occupied intermediate positions between *spoT*^{H414A}
298 and *spoT*^{wt} (**Extended Data Fig. 9a,9b**).

299 Across all suppressors, a core set of genes involved in amino acid metabolism and stress adaptation
300 was consistently restored (**Extended Data Fig. 9c**), whereas genes aberrantly induced in *spoT*^{H414A}
301 cells were broadly repressed (**Extended Data Fig. 9d**). Moreover, strong suppressors (supA and
302 sup41) largely restored expression of acid resistance genes and concomitantly repressed phage
303 shock and SOS response pathways; in contrast, weaker suppressors (supB and sup17) exhibited
304 only partial correction of these transcriptional defects (**Extended Data Fig. 10**), consistent with
305 their physiological phenotypes (**Fig. 5c**).

306 Together, these results indicate that suppressor mutations restore SpoT-dependent regulation in a
307 graded fashion, with transcriptional recovery closely correlating with physiological rescue.

308 **The regulatory function of SpoT H414 is conserved across enteric pathogens**

309 Finally, we asked whether the regulatory role of SpoT H414 is conserved in pathogenic
310 enterobacteria. We introduced the corresponding H414A substitution into SpoT homologs from
311 *Salmonella enterica* serovar Typhimurium and *Shigella flexneri* and expressed these proteins in an
312 *E. coli* ppGpp^0 background.

313 Wild-type SpoT homologs from both species largely restored growth in M9Glc and acid resistance,
314 whereas the corresponding H414A variants failed to support either phenotype (**Fig. 7a-d**). Notably,
315 glutamate supplementation rescued both growth and acid resistance defects in the *Shigella* SpoT$_{sf}$
316 H414A strain but not in the *Salmonella* SpoT$_{st}$ H414A variant. This differential rescue correlated
317 with the extent of sequence divergence within the C-terminal regulatory regions of SpoT. *S. flexneri*
318 SpoT$_{sf}$ differs from *E. coli* SpoT$_{ec}$ at only a single conserved position (A614G) within the CC
319 domain, whereas *S. Typhimurium* SpoT$_{st}$ shares 98.15% overall identity but contains multiple amino
320 acid substitutions distributed across the C-terminal domains, including a cluster of nine

321 substitutions within linker-2 between TGS and CC domains (**Extended Data Fig. 11**). These
322 sequence differences are likely to modulate intramolecular regulatory interactions within SpoT,
323 thereby influencing the ability of the H414A variants to respond to glutamate supplementation, akin
324 to the differential behaviors of the intragenetic suppressor strains (**Fig. 5d**).

325 Altogether, these results demonstrate that SpoT H414 plays a conserved and functionally important
326 role in coordinating growth and acid resistance across enteric pathogens, highlighting the
327 physiological and evolutionary relevance of basal SpoT regulation.

328 **Discussion**

329 **Basal ppGpp defines a distinct regulatory regime coordinating metabolism and stress**
330 **resistance**

331 The stringent response has classically been viewed as an acute adaptation to amino acid starvation,
332 driven by RelA-dependent bursts of ppGpp that globally reprogram transcription and metabolism
333 (**Fig. 7e**, top). In this canonical framework, ppGpp functions as an emergency alarmone that rapidly
334 suppresses growth-associated biosynthetic programs and redirects cellular resources upon severe
335 nutrient limitation.

336 Our findings reveal a complementary and previously underappreciated mode of ppGpp signalling
337 that operates outside this acute starvation paradigm. By dissecting the function of a conserved
338 regulatory residue in SpoT, H414, we identify a basal ppGpp state that is actively maintained during
339 nutrient-limited growth and is essential for coordinating metabolic homeostasis with stress
340 preparedness (**Fig. 7e**, middle). Perturbation of this state uncovers a sharp physiological threshold
341 below which metabolic balance and stress resistance collapse (**Fig. 7e**, bottom).

342 Importantly, the phenotypes observed in *spoT*^{H414A} cells are not readily explained by defects in
343 canonical RelA-mediated stringent response activation. All experiments were conducted in a *ΔrelA*
344 background and under conditions that do not elicit acute amino acid starvation. Moreover, the
345 transcriptional profile of *spoT*^{H414A} cells is fundamentally distinct from those reported in classical
346 stringent response studies driven by RelA-dependent ppGpp bursts[15,16]. Loss of SpoT H414 does
347 not recapitulate either RelA-activated or ppGpp^{0} transcriptional states. Instead, *spoT*^{H414A} cells
348 exhibit a selective and imbalanced response marked by overcommitment to arginine and nucleotide
349 biosynthesis, depletion of central metabolites such as glutamate, and failure to sustain specific
350 stress-response programs, most notably the glutamate-dependent acid resistance system.

351 Together, these observations support the existence of a regulatory regime operating at ppGpp levels
352 above zero yet below the basal state normally maintained by wild-type SpoT. Within this low-
353 amplitude range, ppGpp does not function as a global transcriptional on-off switch, but instead acts
354 as a quantitative tuning signal that constrains metabolic flux allocation and preserves stress
355 preparedness. Loss of this basal control therefore exposes physiological vulnerabilities that are not
356 captured by classical models of the stringent response. In this framework, SpoT functions not
357 merely as a modulator of RelA activity, but as a primary regulator of a stabilized physiological
358 state. This low but non-zero ppGpp levels act not as an emergency brake on growth, but as a
359 buffering signal that integrates metabolism with stress preparedness during nutrient-limited growth.

360 **SpoT-mediated control of glutamate homeostasis underlies stress preparedness without**
361 **compromising basal viability**

362 A central mechanistic insight from this study is that SpoT-dependent basal ppGpp constrains
363 metabolic flux allocation to preserve glutamate homeostasis. Transcriptomic profiling of *spoT*^{H414A}
364 cells revealed coordinated induction of arginine biosynthesis (**Fig. 3a,b**), which directly consumes

365 glutamate, together with upregulation of *de novo* purine nucleotide biosynthesis (**Extended Data**
366 **Fig. 3a,b**), which indirectly increases glutamate demand through enhanced glutamine utilization.
367 This pattern reflects a loss of quantitative control over anabolic commitment rather than selective
368 activation of a single biosynthetic pathway.

369 Genetic and physiological analyses identify arginine biosynthesis as the primary driver of glutamate
370 depletion in this context. Blocking the first committed step of arginine synthesis prevents glutamate
371 starvation and restores growth (**Fig. 3d**), whereas forced arginine overproduction phenocopies the
372 $spoT^{H414A}$ defect (**Fig. 3e**).

373 Glutamate occupies a uniquely central position in bacterial physiology, serving both as a metabolic
374 hub and as the essential substrate for the glutamate-dependent Gad acid resistance system.
375 Accordingly, glutamate depletion provides a parsimonious explanation for the coupled phenotypes
376 observed in $spoT^{H414A}$ cells, including impaired growth in minimal medium and failure of acid
377 resistance. Glutamate supplementation and GadE-dependent activation of the acid resistance
378 program rescue survival under low-pH challenge (**Fig. 4a; Extended Data Fig. 4b**), indicating that
379 SpoT-dependent basal ppGpp enforces a metabolic prioritization strategy that preserves metabolites
380 required for effective stress defence.

381 Importantly, disruption of this basal regulatory state does not cause immediate loss of viability
382 under neutral, well-buffered conditions (**Extended Data Fig. 1g)**, despite severe repression of acid
383 resistance genes and extreme sensitivity to low pH (**Fig. 2c**). This separation between basal growth
384 capacity and stress survival indicates that SpoT-derived basal ppGpp primarily maintains
385 physiological preparedness rather than minimal viability. This distinction helps explain why the
386 most pronounced phenotypes of $spoT^{H414A}$ cells emerge only upon environmental challenge.

387 Notably, RelA is dispensable for acid resistance under the conditions examined (**Fig. 2c**),
388 highlighting a functional division of labour between the two stringent response enzymes. Whereas
389 RelA mediates acute, high-amplitude responses to amino acid starvation, SpoT maintains a low-
390 level regulatory state that buffers metabolic allocation and supports long-term stress readiness.

391 **SpoT maintains basal ppGpp through coupled activity tuning and abundance feedback**

392 The identification of intragenic suppressors of *spoT*^{H414A} reveals that SpoT encodes an intrinsic
393 regulatory system capable of quantitatively tuning basal ppGpp levels. Suppressor mutations
394 distributed across both the catalytic and regulatory regions of SpoT restore growth (**Fig. 5c**) and
395 acid resistance (**Fig. 5d**) without producing large, readily detectable increases in ppGpp (**Fig. 6a**).
396 These observations indicate that physiological rescue does not require restoration of wild-type
397 ppGpp abundance, but instead depends on re-establishing a narrowly defined sub-basal ppGpp
398 state , consistent with the graded restoration of transcriptional programs observed across suppressor
399 strains (**Extended Data Fig. 9,10**).

400 Direct perturbation of SpoT enzymatic activities supports this interpretation. Inactivation of ppGpp
401 synthesis abolishes suppressor-mediated growth recovery (**Fig. 6b**), whereas inactivation of SpoT
402 hydrolase activity leads to substantial ppGpp accumulation (**Fig. 6c**) and accelerated growth
403 resumption (**Fig. 6d**). These results indicate that suppressor mutations rebalance SpoT synthetic and
404 hydrolytic activities rather than bypassing the requirement for ppGpp. The inability to construct
405 synthetase-only variants in specific suppressor backgrounds further underscores the importance of
406 quantitative control. In these contexts, elevated ppGpp levels are likely deleterious, consistent with
407 the well-established growth-inhibitory effects of excessive ppGpp. Thus, both insufficient and
408 excessive ppGpp are incompatible with optimal growth, defining a sharply constrained
409 physiological window for basal ppGpp function.

410 However, tuning of catalytic activity alone is unlikely to be sufficient to stabilize a low-amplitude
411 signalling state over extended periods of growth. Consistent with this, SpoT protein levels are
412 markedly elevated in *spoT*^{H414A} cells but reduced in suppressor backgrounds (**Fig. 6e**), revealing an
413 additional layer of regulation mediated by negative feedback on SpoT abundance. This inverse
414 relationship suggests that basal ppGpp limits SpoT accumulation, thereby constraining total
415 enzymatic capacity for ppGpp turnover.

416 Together, quantitative tuning of SpoT catalytic activity and feedback control of SpoT abundance
417 may enable precise maintenance of ppGpp within a narrow functional window. This coupled
418 regulatory architecture provides a mechanistic model for how bacteria stabilize a low-level ppGpp
419 signalling state sufficient for metabolic coordination and stress preparedness, yet below the
420 threshold that triggers growth arrest and the canonical stringent response.

421 **Conservation and implications of basal SpoT regulation**

422 The functional conservation of H414 across *Escherichia coli*, *Salmonella*, and *Shigella* SpoT
423 proteins demonstrates that this residue is broadly required for growth in minimal medium and
424 survival under extreme acid stress (**Fig. 7a-d**). At the same time, the differential ability of
425 *Salmonella* and *Shigella* SpoT H414A variants to respond to glutamate supplementation, akin to the
426 intragenetic suppressors (**Fig. 5d**), suggests that sequence divergence within C-terminal regulatory
427 regions modulates how basal SpoT regulation is implemented across species.

428 These observations indicate that, while the requirement for SpoT-mediated basal ppGpp control is
429 conserved, individual bacteria may tune SpoT regulatory domains to optimize metabolic and stress-
430 response coordination according to their metabolic capacity, ecological niches and life cycles. In
431 this framework, basal ppGpp does not represent a rigid or uniform signalling state, but rather a

432 conserved regulatory principle flexibly adapted through species-specific intramolecular tuning of
433 SpoT.

434 Several important questions remain, including the nature of the signal sensed by SpoT H414 and the
435 absolute intracellular concentrations and temporal dynamics of basal ppGpp. Addressing these
436 questions will require new approaches capable of resolving low-abundance alarmone pools with
437 high sensitivity, ideally at single-cell resolution, and across diverse growth conditions and bacterial
438 species. Elucidating how basal ppGpp selectively modulates distinct metabolic and stress-response
439 pathways will further clarify how this regulatory regime integrates diverse physiological demands.

440 Given the central role of acid resistance in enteric pathogenesis, SpoT-mediated basal ppGpp
441 regulation may represent a previously underappreciated vulnerability that could be exploited to
442 compromise bacterial survival under host-associated stresses.

443 **Figures and legends**

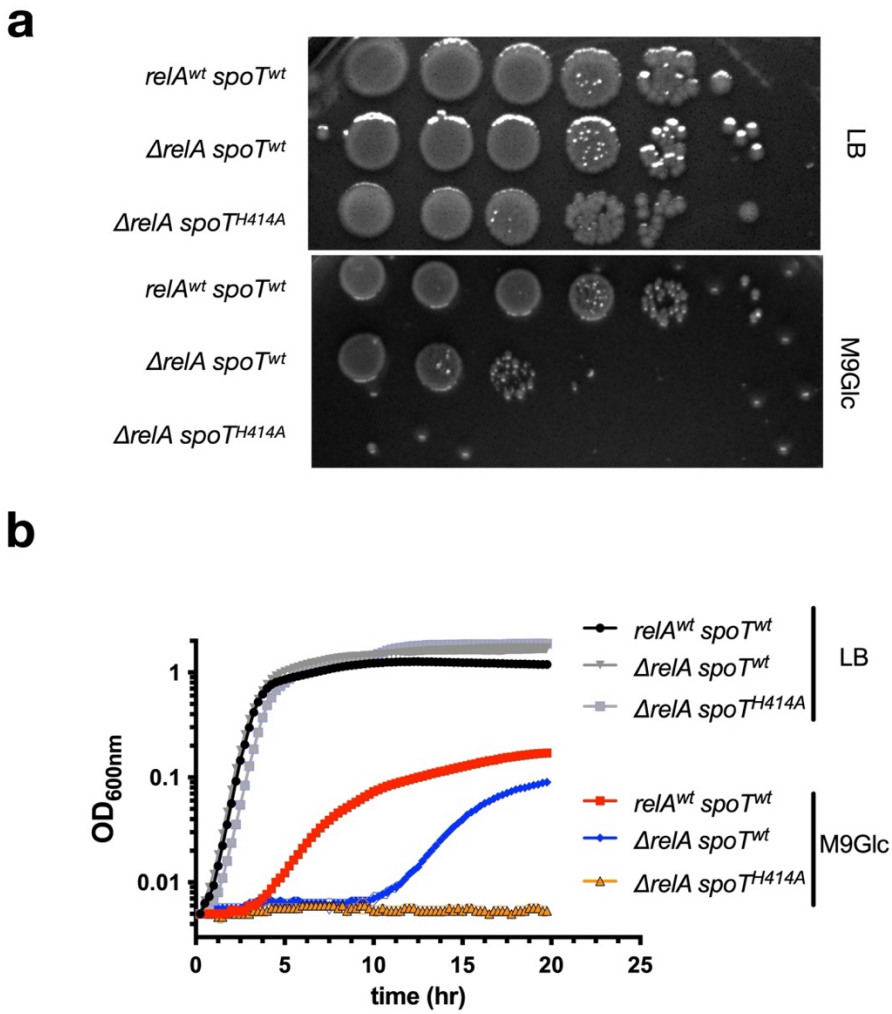

444

445 **Figure 1. A conserved SpoT H414A mutation reveals defective growth on M9Glc medium. (a)**

446 Growth of wild type *E. coli* MG1655 (*relA*^{wt} *spoT*^{wt}), and Δ*relA spoT*^{wt}, Δ*relA spoT*^{H414A} strains on

447 LB and M9Glc solid media. **(b)** Growth dynamics of the same strains in liquid LB and M9Glc media.

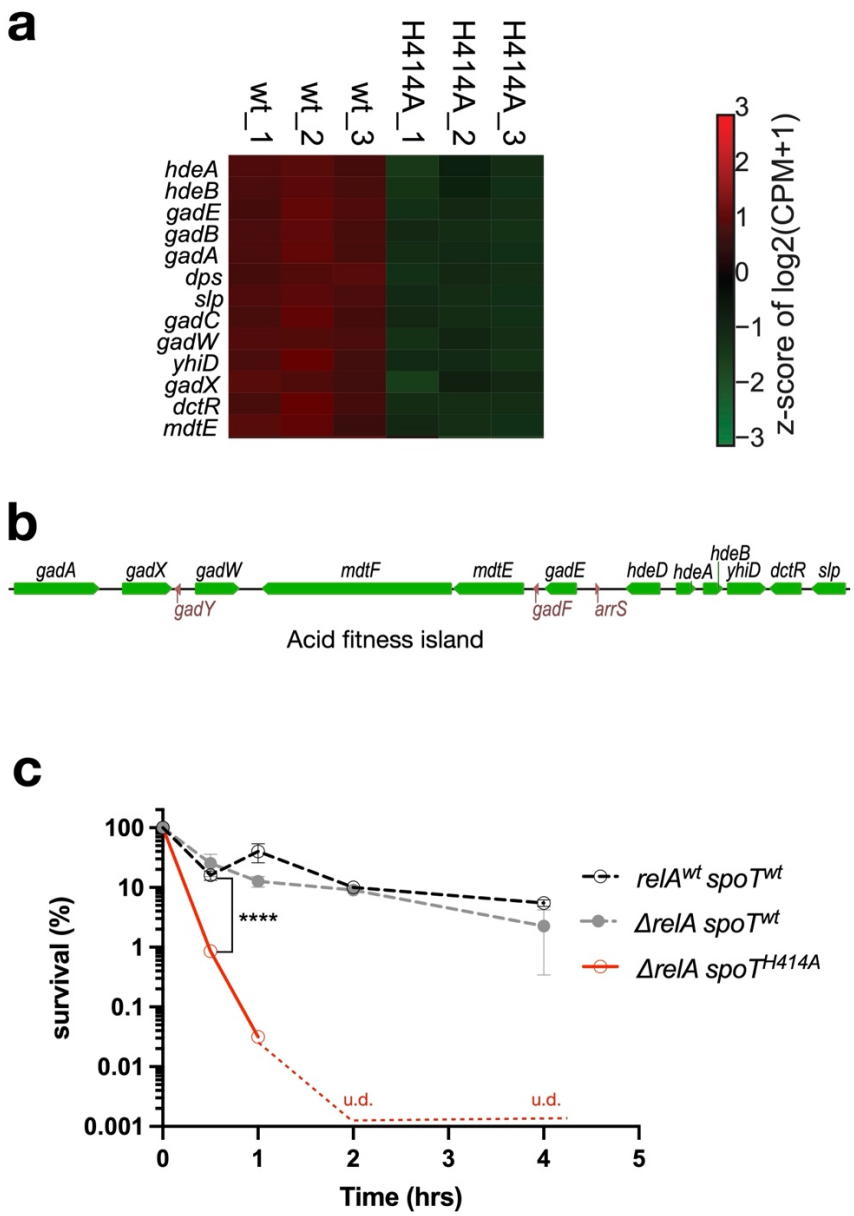

Figure 2. Transcriptomic analysis reveals collapse of acid resistance programs. (a) Heatmap of genes encoded in the *E. coli* acid fitness island in *spoT*^{H414A} relative to *spoT*^{wt}. **(b)** Genetic organization of the *E. coli* acid fitness island. (**c**) Acid resistance assay of wild type MG1655 (*relA*^{wt} *spoT*^{wt}), Δ*relA spoT*^{H414A} and Δ*relA spoT*^{wt}. Survival of indicated strains following challenge at pH 2.5, expressed as the percentage of survival (i.e., colony-forming units (CFUs) remaining relative to starting CFUs) for each strain. Data are means ± s.d. from biological replicates. u.d., undetectable.

455 Statistical significance was assessed using unpaired two-tailed Student's *t*-tests. **** denote $P <$

456 0.0001.

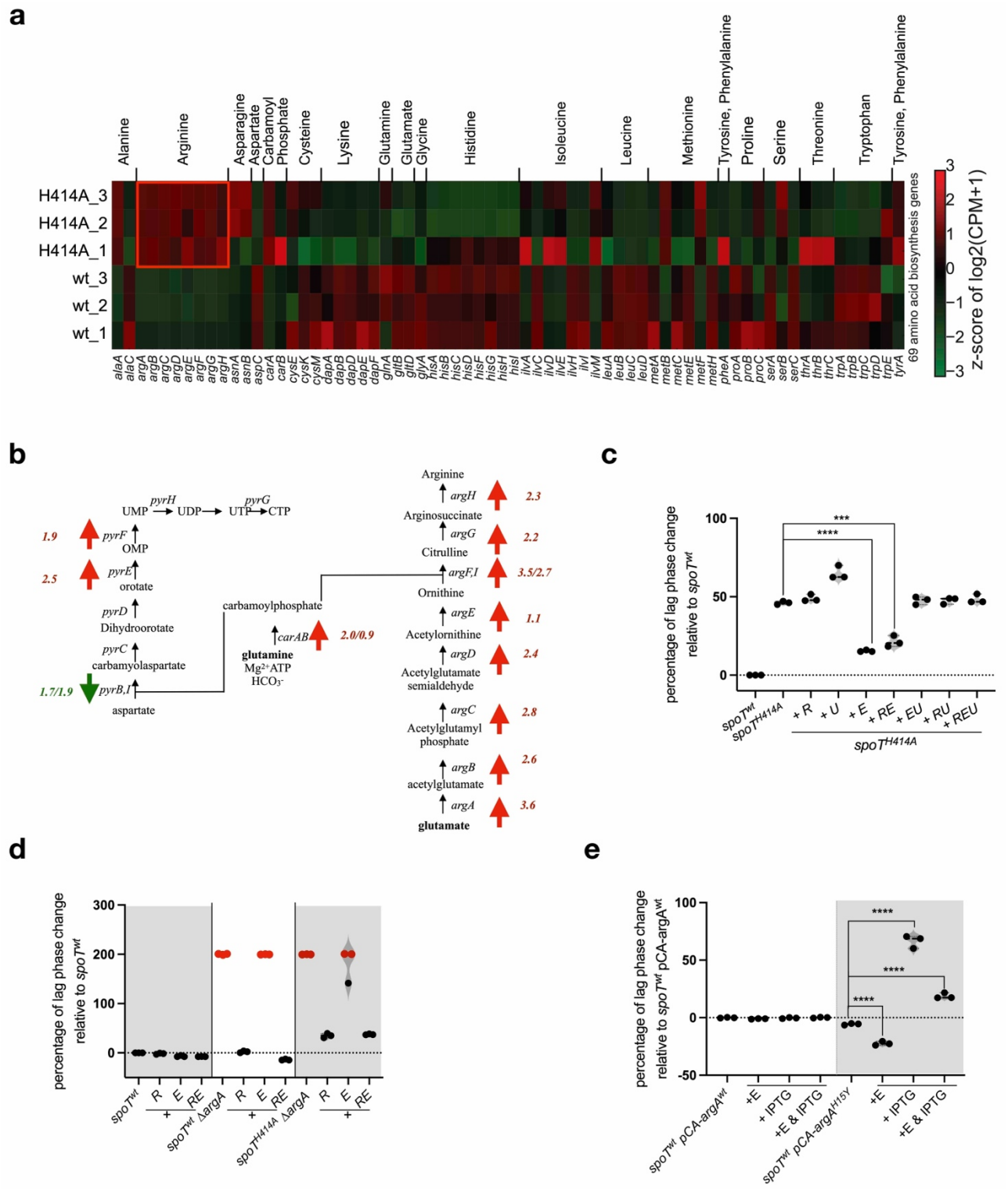

457

458 **Figure 3. Arginine metabolic overflow drives glutamate depletion in *spoT^{H414A}*. (a)** Heatmap of
459 genes involved in amino acid biosynthesis, comparing *spoT^{H414A}* and *spoT^{wt}* strains. The arginine
460 biosynthesis genes are highlighted. **(b)** Schematic of the arginine biosynthesis pathway in *E. coli*.
461 Genes upregulated in *spoT^{H414A}* cells are indicated by red upward arrows, accompanied by average
462 $\log_2$ fold-change values relative to *spoT^{wt}*. **(c)** Normalized lag phase duration of *spoT^{H414A}* cells
463 grown in M9Glc medium with supplementation of arginine (5.2 mM, R), uracil (0.2 mM, U),
464 glutamate (0.6 mM, E), or the indicated combinations, expressed relative to the *spoT^{wt}* strain. **(d)**
465 Normalized lag phase duration of indicated strains grown in M9Glc medium with supplementation
466 of arginine (R), glutamate (E), or both, relative to *spoT^{wt}*. Red dots indicate failure to resume
467 growth within the 72-h observation window. **(e)** Normalized lag phase duration of *spoT^{wt}* strains
468 harboring pCA24N-*argA^{wt}* or the feedback-resistant pCA24N- *argA^{H15Y}* allele, grown with or
469 without IPTG induction and/or glutamate supplementation (0.6 mM), relative to the uninduced
470 *argA^{wt}* control. Data are means ± s.d. from biological replicates. Statistical significance was
471 assessed using unpaired two-tailed Student's *t*-tests. ****, *** denote $P < 0.0001$ and 0.001,
472 respectively.

473

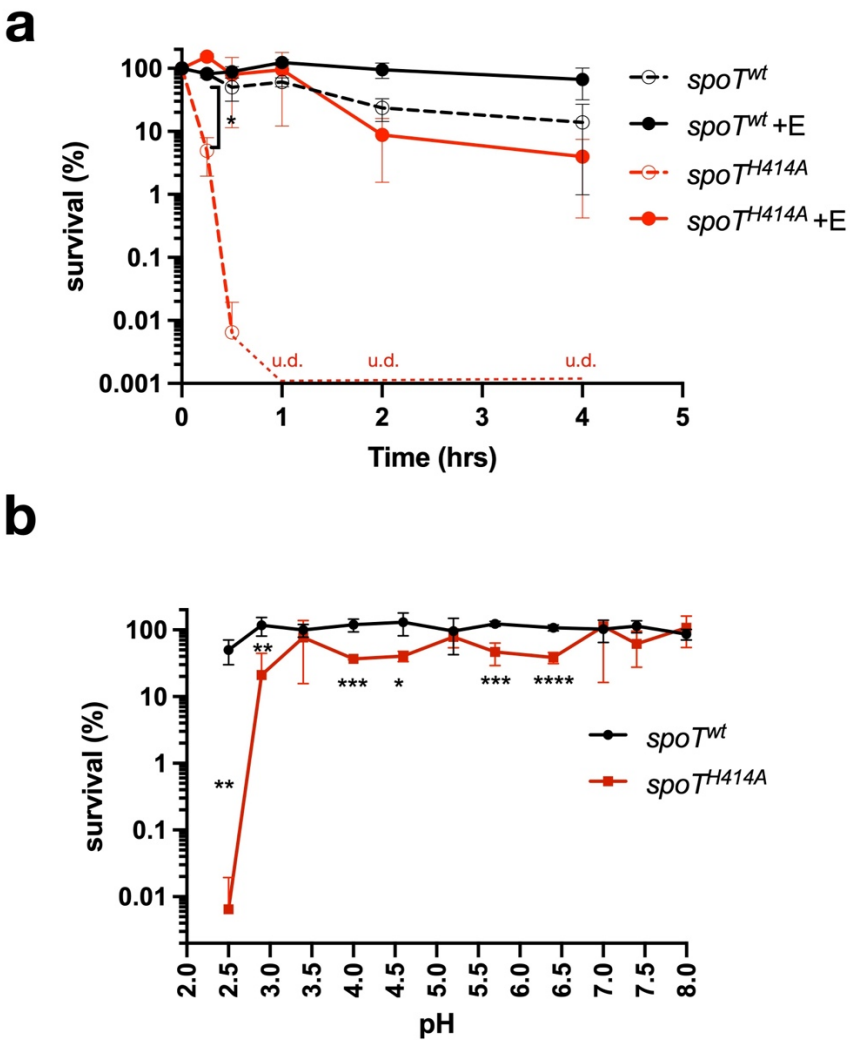

474

475 **Figure 4. SpoT H414 is required for survival under extreme acid stress.**

476 **(a)** Acid resistance assay of Δ*relA spoT*^{H414A} and Δ*relA spoT*^{wt} as in Figure 2c. Where indicated

477 (+E), glutamate (0.6 mM) was included in the acid challenge medium. u.d., undetectable. **(b)**

478 Survival of *spoT*^{H414A} and *spoT*^{wt} strains following 30 min challenge in buffers adjusted to the

479 indicated pH values, normalized to starting CFUs. Data are means ± s.d. from biological replicates.

480 Statistical significance was assessed using unpaired two-tailed Student's *t*-tests. ****, ***, **, *

481 denote $P < 0.0001$, 0.001, 0.01, and 0.05, respectively.

482

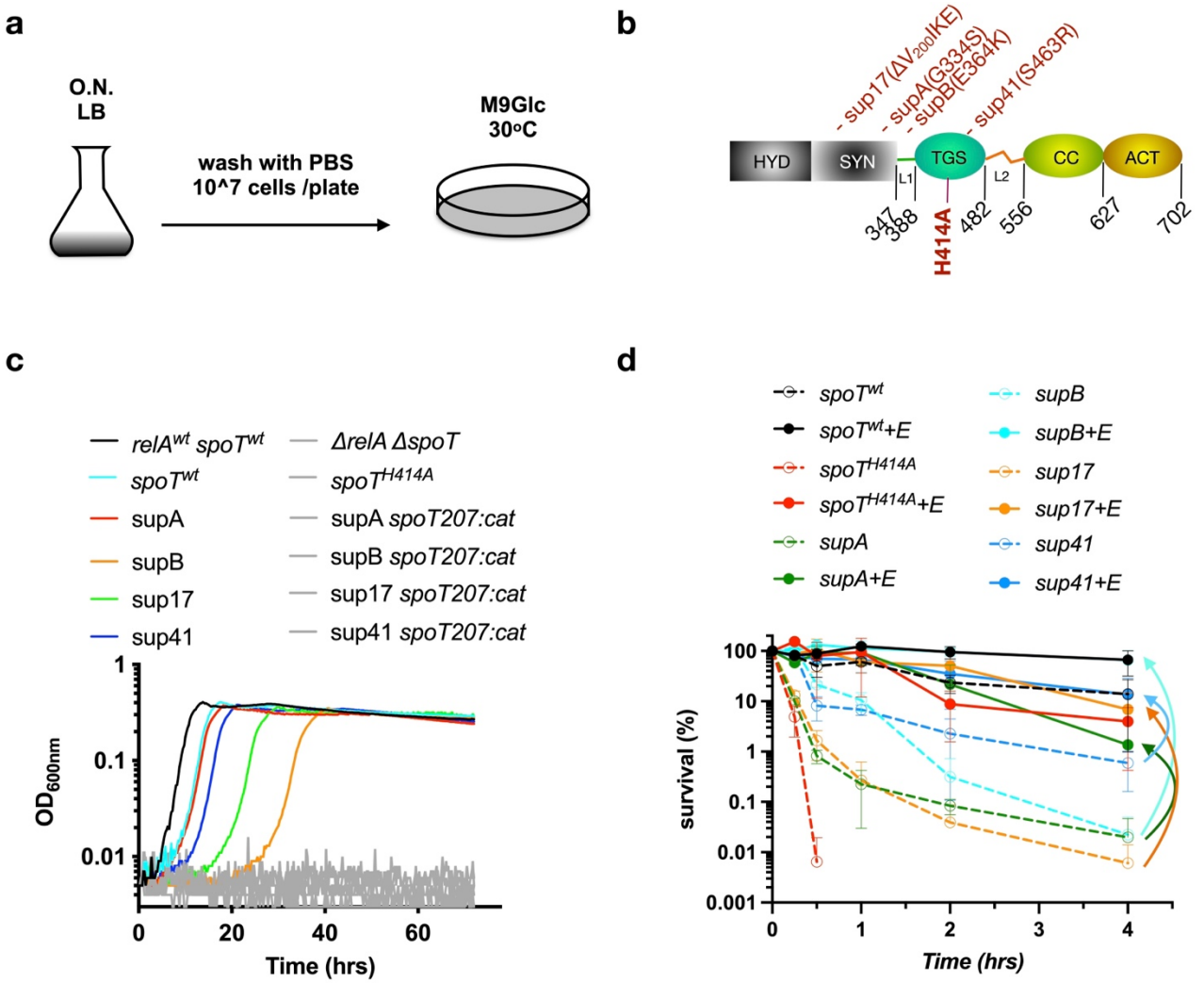

483

484 **Figure 5. Intragenic SpoT suppressor mutations restore growth and acid resistance. (a)**
485 Schematic illustrating the isolation of spontaneous suppressor mutations that enable growth of
486 *spoT*^{H414A} cells on M9Glc medium. **(b)** Domain architecture of the SpoT protein, indicating the
487 locations of suppressor mutations. Amino-acid positions are shown below. L1/L2, linker-1/linker-2;
488 HYD, hydrolase domain; SYN, synthetase domain; TGS, ThrRS-GTPase-SpoT domain; CC,
489 conserved cysteine domain; ACT, aspartate kinase-chorismate mutase-TyrA domain. **(c)** Growth
490 dynamics of four suppressor strains (supA, supB, sup17, sup41) compared with *spoT*^{H414A}, *spoT*^{wt},
491 ppGpp^0 (*ΔrelA ΔspoT*), and wild-type MG1655 (*relA*^{wt} *spoT*^{wt}). Also shown are suppressor strains
492 in which *spoT* was deleted (*spoT207::cat*). **(d)** Survival of indicated strains following challenge at

493 pH 2.5. Where indicated (+E), glutamate (0.6 mM) was included. Data are means ± s.d. Statistical
494 significance was assessed using unpaired two-tailed Student's *t*-tests. ***, **, * denote $P < 0.001$,
495 0.01, and 0.05, respectively.

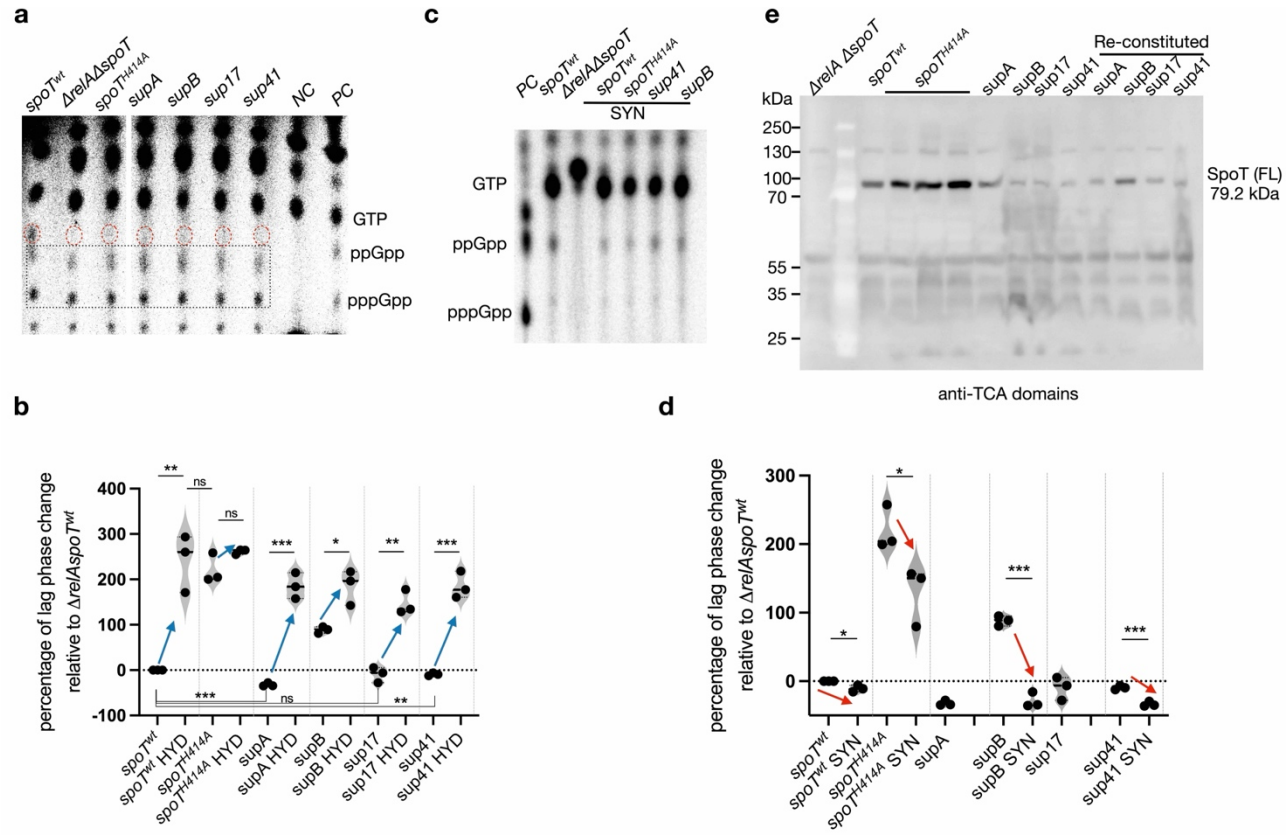

496

497 **Figure 6. A sub-basal ppGpp pool is sufficient for physiological function. (a)** Thin-layer
498 chromatography (TLC) analysis of ^{32}p-labeled nucleotides from indicated strains grown in low-
499 phosphate MOPS minimal medium supplemented with 0.2% glucose. NC and PC denote valine-
500 treated *ΔrelA ΔspoT* and wild-type MG1655 controls, respectively. Red circles mark ppGpp; boxed
501 regions indicate nonspecific spots also present in *ΔrelA ΔspoT* samples. **(b)** Effect of inactivating
502 SpoT ppGpp synthetase activity (E319Q; HYD) on growth recovery in M9Glc. Lag phase duration
503 is normalized to *spoT*^{wt}. **(c)** TLC analysis of ^{32}p-labeled nucleotides from strains carrying SpoT
504 hydrolase-inactive mutations (H72A D73A; SYN). **(d)** Growth recovery of hydrolase-inactive
505 strains (SYN), quantified as normalized lag phase duration relative to *spoT*^{wt}. Note that the

506 hydrolase-inactive (SYN) variants of supA and sup17 could not be obtained, thereby not tested. **(e)**
507 Immunoblot analysis of SpoT protein levels using an antiserum raised against the SpoT C-terminal
508 (TGS-CC-ACT; anti-TCA) region. Cells were grown in M9Glc to early exponential phase (OD_{600nm}
509 ≈ 0.2) prior to sampling. *spoT*^{H414A} samples were collected after prolonged incubation, as in
510 Extended Data Fig. 1c. *ΔrelA ΔspoT* cells grown in LB served as a negative control.

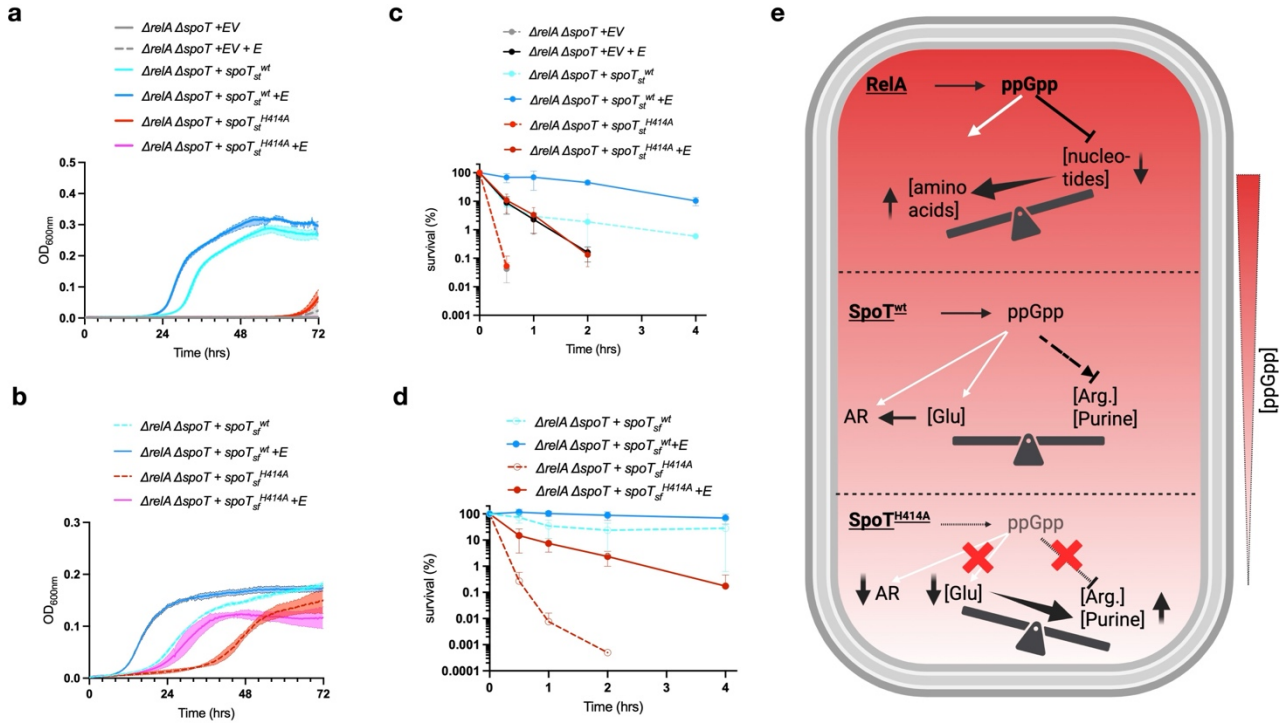

511

512 **Figure 7. Conservation of SpoT H414 function and model for basal ppGpp regulation. (a,b)**
513 Growth of *E. coli* ppGpp^0 strains complemented with SpoT homologs from *Salmonella enterica*
514 serovar Typhimurium ($SpoT_{st}$) (**a**) or *Shigella flexneri* ($SpoT_{sf}$) (**b**). E, glutamate (0.6 mM); EV,
515 empty vector. Data represent at least three biological replicates. **(c,d)** Survival of complemented
516 ppGpp^0 strains expressing $SpoT_{st}$ (**c**) or $SpoT_{sf}$ (**d**)) following challenge at pH 2.5, normalized to
517 starting CFUs. Where indicated (+E), glutamate (0.6 mM) was included. **(e)** Top: Under acute
518 amino-acid starvation, RelA is rapidly activated by ribosome-associated signals to generate a high-
519 amplitude ppGpp surge, globally reprogramming transcription and metabolism to suppress

520 nucleotide pathways and promote amino-acid availability. Middle: SpoT maintains a low but
521 physiologically essential basal ppGpp pool that is distinct from and independent of RelA. This basal
522 ppGpp state coordinates metabolic homeostasis by restraining excessive arginine and purine
523 biosynthesis, preserving intracellular glutamate levels, and priming multiple acid resistance
524 programs, including the glutamate-dependent Gad system (AR). Bottom: In *spoT*^{H414A} cells, a sub-
525 basal level of ppGpp remains below the threshold required for effective metabolic and stress
526 control. Therefore, arginine and purine biosynthetic pathways become overactivated, intracellular
527 glutamate is depleted, and acid resistance programs are inadequately induced, resulting in growth
528 failure in minimal medium and extreme sensitivity to acid stress.

529

530 **EXTENDED DATA FIGURE LEGENDS**

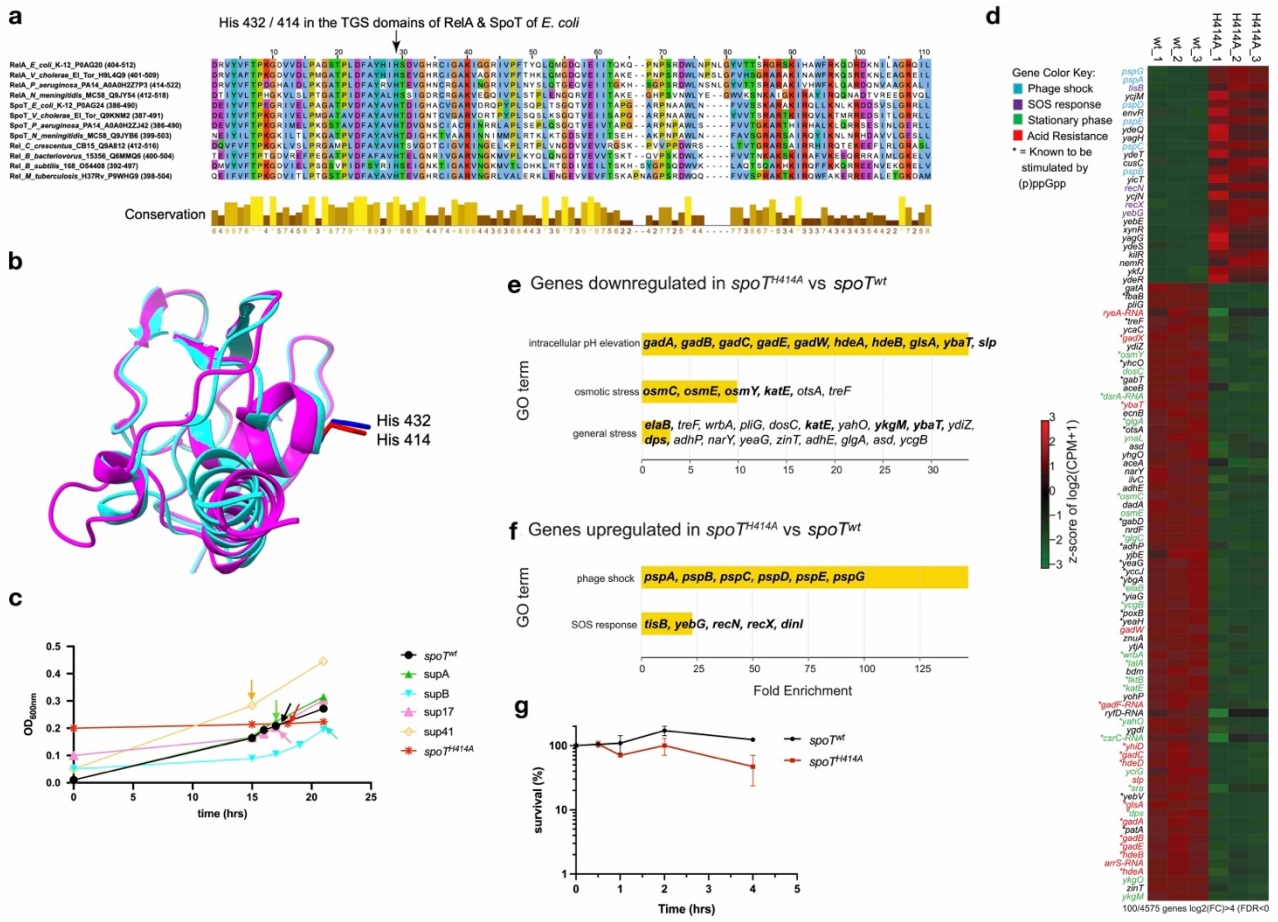

531

532 **Extended Data Fig. 1 (a)** Sequence alignment of 12 TGS domains of RelA, SpoT and their
533 homologous proteins from α, β, γ and δ proteobacteria, Firmicute and Actinomycete. The highly
534 conserved position corresponding to His 432 of RelA and 414 of SpoT of *E. coli* is indicated with
535 an arrow. **(b)** Superpositioning of the TGS domains of RelA and SpoT from *E. coli* (rmsd over 91
536 of 98 atom pairs is 0.762 Å) generated by AF3. **(c)** Representative growth curves of Δ*relA*
537 *spoT*^{H414A}, Δ*relA spoT*^{wt} and the four suppressor strains in M9Glc media for collecting RNA
538 sequencing samples. Cells were collected when their OD_{600nm} approach ca. 0.2, except for *spoT*^{H414A}
539 cells, which could not grow in this medium, thus these cells were collected after incubated for 18
540 hrs in the same medium. Coloured arrows indicate the sampling points for each strain. **(d)** Heatmap

541 of genes with greater than 16-fold changes between Δ*relA spoT*^{H414A} and Δ*relA spoT*^{wt} cells growing
542 in M9Glc medium. **(e)** Gene ontology groups of genes downregulated in the *spoT*^{H414A} strain.
543 Genes downregulated at least 16-fold were extracted using DEGUST (|Log2(FC)| > 4; FDR < 0.05)
544 and analysed by AmiGO and Panther. The 58 genes downregulated more than 16-fold (Log2(FC) <
545 -4) are listed in **Table S3**. **(f)** Gene ontology groups of genes upregulated at least 16-fold in the
546 *spoT*^{H414A} strain. The 28 genes upregulated more than 16-fold (Log2(FC) > 4) are listed in **Table**
547 **S3**. Note the differences in the Fold Enrichment scales in **(e)** and **(f)**. Gene names in bold in (**e, f**)
548 are strongly up or downregulated. **(g)** Normalized percentage of surviving viable cells of the *spoT*^{wt}
549 and *spoT*^{H414A} strains growing in M9Glc medium. Two replicates were performed and presented.

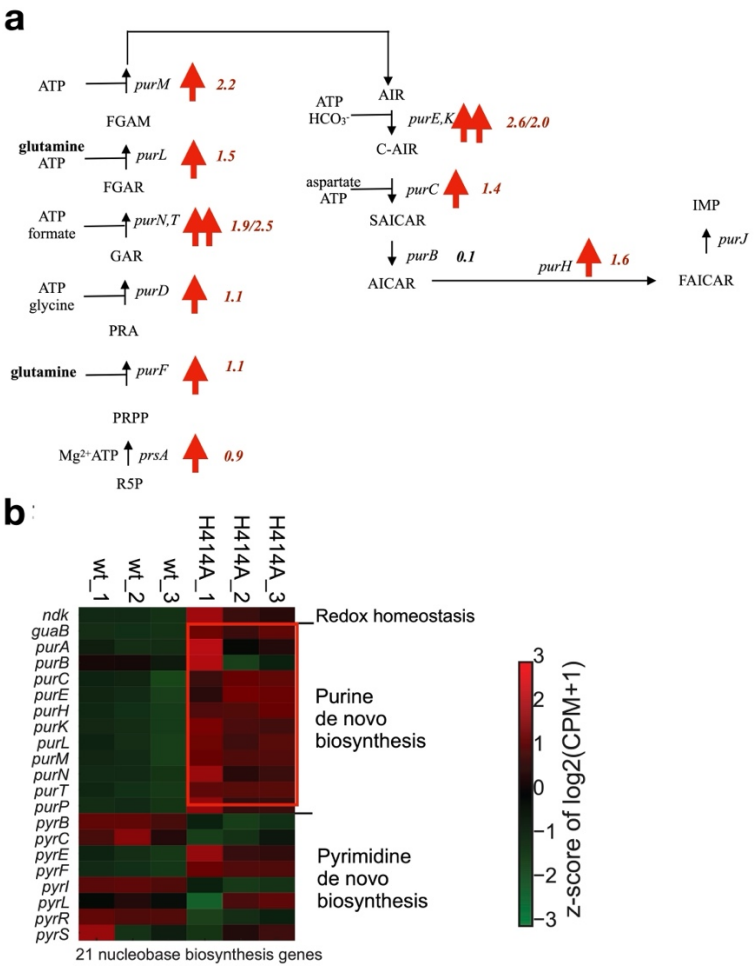

550

551 **Extended Data Fig. 2 (a)** Purine nucleotide de novo biosynthesis pathway in *E. coli*. The
552 upregulated genes are indicated by a red upward arrow alongside average log2(FC) values of
553 *spoT*^{H414A} versus *spoT*^{wt}. R5P, ribose-5-phosphate; PRPP, 5-phosphoribosyl 1-pyrophosphate; PRA,
554 5-phosphoribosylamine; GAR, 5'-phosphoribosylglycinamide; FGAR, 5'-phosphoribosyl-N-
555 formylglycineamide; FGAM, 5'-phosphoribosylformylglycinamidine; AIR, 5-aminoimidazole
556 ribonucleotide; C-AIR, 5-carboxyamino-1-(5-phospho-D-ribosyl)imidazole; SAICAR, 1-(5-
557 phosphoribosyl)-4-(N-succino-carboxamide)-5-aminoimidazole; AICAR, 5-amino-1-(5-phospho-D-
558 ribosyl)imidazole-4-carboxamide; FAICAR, 5-formamido-1-(5-phospho-D-ribosyl)imidazole-4-
559 carboxamide; IMP, inosine 5'- monophosphate. **(b)** Heatmap of genes involved in purine and
560 pyrimidine nucleotide de novo biosynthesis. The red box indicates purine de novo biosynthesis
561 genes.

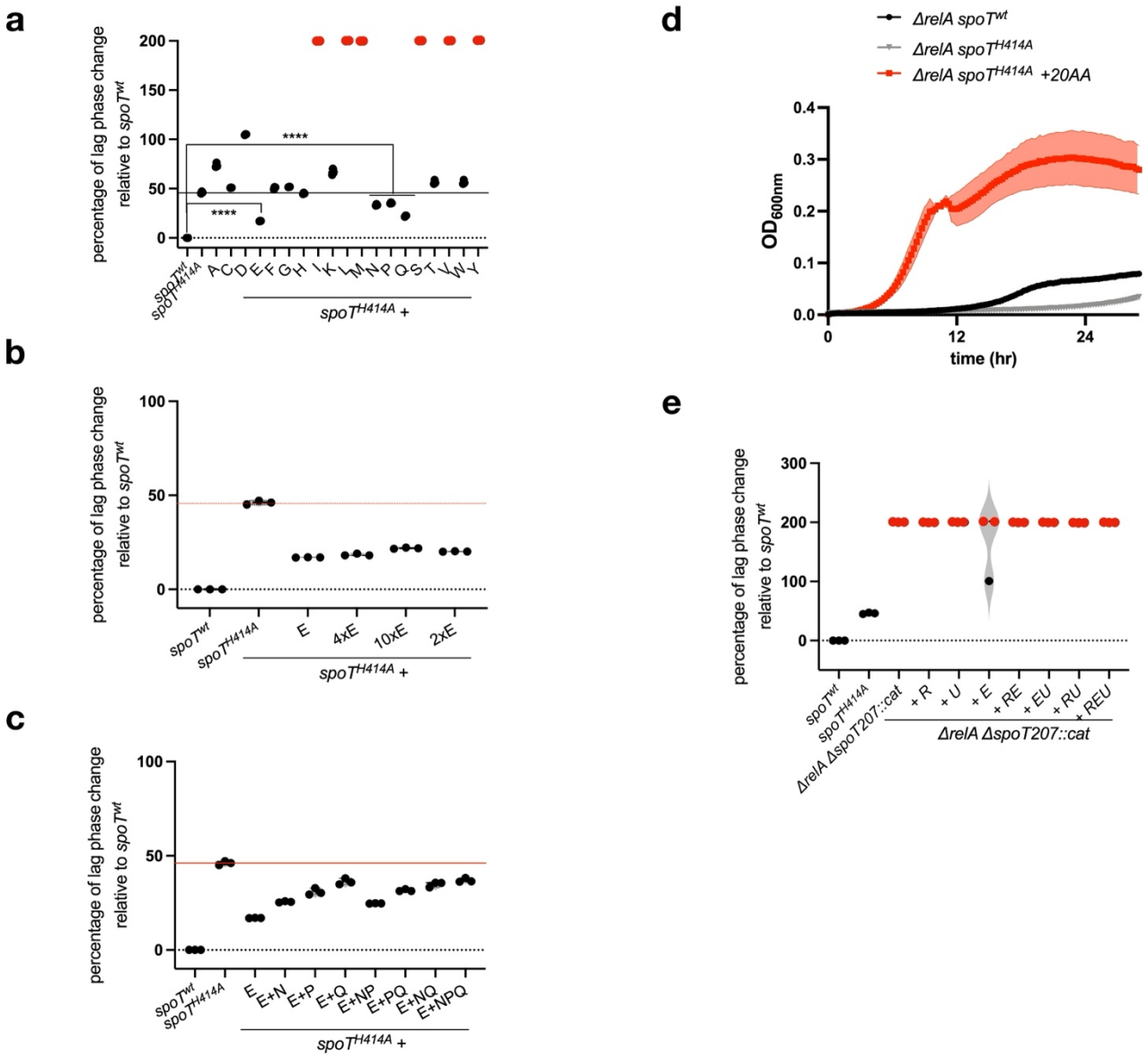

562

563 **Extended Data Fig. 3 (a)** Normalized lag phase length of the *spoT*^{H414A} strain without or with
564 supplemented each of the 20 amino acids (in single letters; A, alanine 0.8mM; C, cysteine 0.1mM;
565 D, aspartic acid 0.4mM; E, glutamate 0.6mM; F, phenylalinine 0.4mM; G, glycine 0.8mM; H,
566 histidine 0.2mM; I, isoleucine 0.4mM; K, lysine 0.4mM; L, leucine 0.8mM; M, methionine 0.2mM;
567 N, asparigine 0.4mM; P, proline 0.4mM; Q, glutamine 0.6mM; R, arginine 5.2mM; S, serine 10mM;
568 T, threonine 0.4mM; V, valine 0.6mM; W, tryptophan 0.1mM; Y, tyrosine 0.2mM), relative to the
569 *spoT*^{wt} strain in M9Glc medium. **(b)** Normalized lag phase length of the *spoT*^{H414A} strain without or

570 with supplemented 1x, 2x, 4x, 10x glutamate (E, 1x = 0.6 mM), relative to the *spoT*^{wt} strain in M9Glc
571 medium. **(c)** Normalized lag phase length of the *spoT*^{H414A} strain without or with supplemented
572 glutamate (0.6 mM) together with glutamine (Q, 0.6 mM), proline (P, 0.4 mM), asparagine (N, 0.4
573 mM), relative to the *spoT*^{wt} strain in M9Glc medium. **(d)** Representative growth curves of Δ*relA*
574 *spoT*^{H414A}, Δ*relA spoT*^{wt} strains without or with all 20 amino acids (+20AA) (see method for details)
575 in M9Glc medium. Two biological replicates each with two technical replicates were performed and
576 presented. **(e)** Normalized lag phase length of the Δ*relA*Δ*spoT207::cat* (ppGpp^0) strain without or
577 with supplemented arginine (5.2 mM, R), uracil (0.2 mM, U), glutamate (0.6 mM, E) or their varied
578 combinations, relative to the *spoT*^{wt} strain in M9Glc medium. Red dots indicate fails of regrowth
579 within the tested time range of 72 hrs.

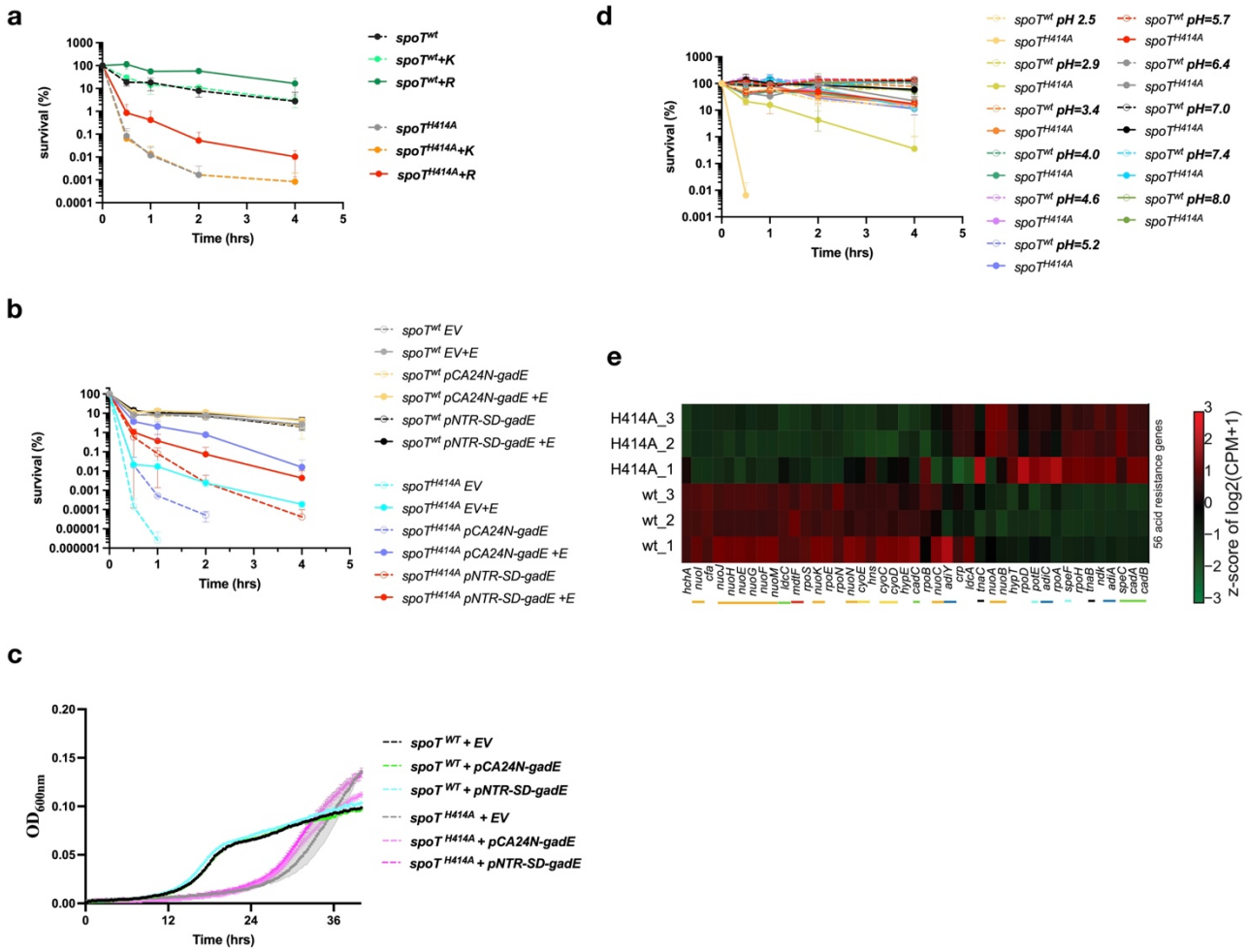

580

581 **Extended Data Fig. 4 (a)** Normalized percentage of surviving cells of various strains after
582 challenged with pH=2.5. The data were normalized to the starting CFUs of each respective tested
583 strain. +K, +R, lysine (0.6 mM), arginine (0.6 mM) included in the pH=2.5 medium, respectively.
584 **(b)** Normalized percentage of surviving cells of *spoT*^{wt} or *spoT*^{H414A} strains containing various
585 plasmid vectors (pCA24N [42], pNTR-SD [43]) after challenged with pH=2.5. The data were
586 normalized to the starting CFUs of each respective tested strain. EV, empty vector pCA24N. +E,
587 glutamate (0.6 mM) included in the pH=2.5 medium. **(c)** Representative growth curves of *spoT*^{H414A}
588 and *spoT*^{wt} strains containing either the empty vector (EV) or a *gadE* gene on pCA24N or pNTR-SD
589 vectors in M9Glc medium. Two biological replicates each with two technical replicates were
590 performed and presented. **(d)** Normalized percentage of surviving cells of *spoT*^{wt} and *spoT*^{H414A}
591 strains after challenged with media of various pH values. The data were normalized to the starting
592 CFUs of each respective tested strain. **(e)** Heatmap of genes involved in acid resistance. Colored
593 bars indicate genes belonging to the same acid resistance systems: orange, *nuo* genes encoding
594 NADH dehydrogenase I; yellow, *cyo* genes encoding cytochrome *bo* oxidase; green, lysine
595 dependent acid resistance systems; cyan, ornithine dependent acid resistance system; black, alkaline
596 stress; dark blue, arginine dependent acid resistance system.

597 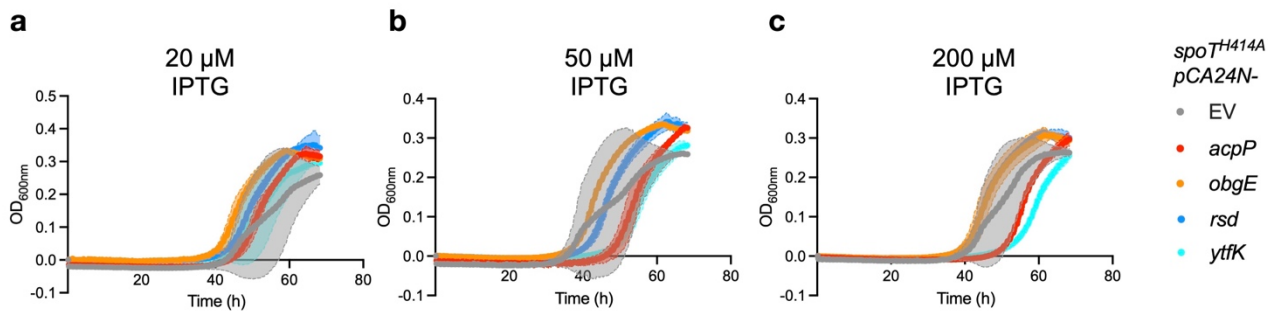

598 **Extended Data Fig. 5. Growth dynamics of *spoT*^{H414A} strains expressing candidate SpoT**
599 **regulators.**

600 Growth curves of *spoT*^{H414A} strains carrying either the empty vector (EV) pCA24N or pCA24N

601 derivatives expressing *acpP, obgE, rsd,* or *ytfK*. Cells were grown in M9Glc medium supplemented

602 with the indicated concentrations of IPTG to induce expression of the respective genes. Data

603 represent the mean ± s.d. from three independent biological replicates.

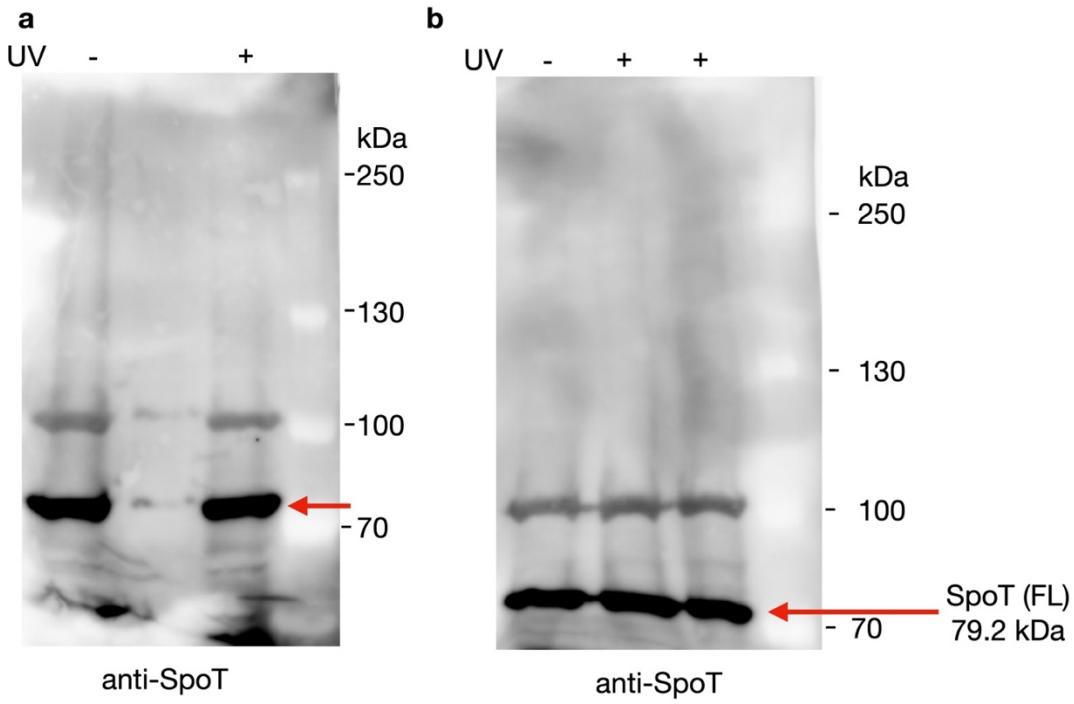

604

605 **Extended Data Fig. 6. Western blot analysis of SpoT following unnatural amino acid-**

606 **mediated UV crosslinking.**

607 SpoT carrying a photo-crosslinkable unnatural amino acid at position 414 was expressed in a *ΔrelA*

608 *ΔspoT* background and subjected to UV irradiation (365 nm) to induce covalent crosslinking to

609 proximal proteins. Samples collected in the absence (-) or presence (+) of UV irradiation were

610 analyzed by SDS-PAGE and immunoblotting using anti-SpoT antiserum. Two independent

611 representative experiments are shown (**a, b**). The positions of full-length SpoT are indicated by the

612 red arrows.

613

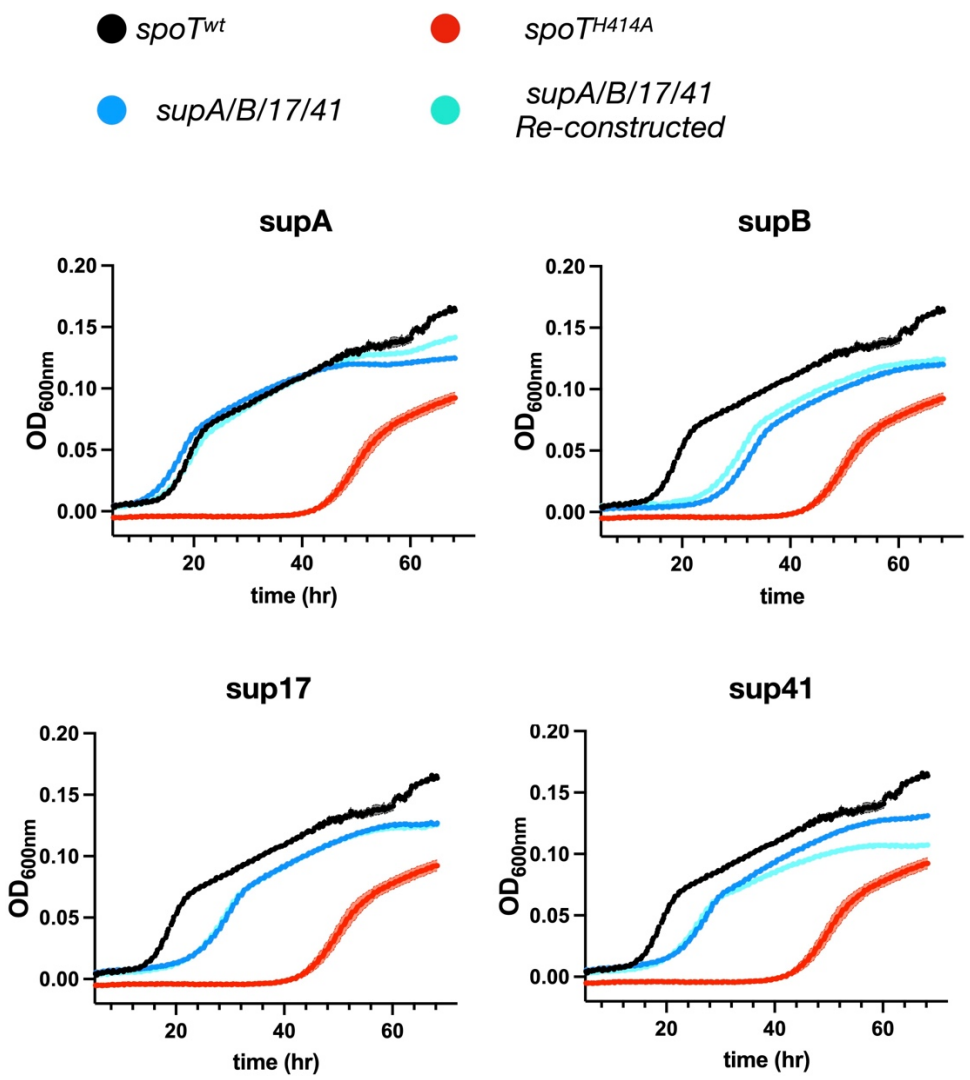

614

615 **Extended Data Fig. 7** Growth dynamics of re-constructed four suppressors (cyan)

616 (*supA/supB/sup17/sup41*) in comparison to *spoT*^{H414A}, *spoT*^{wt}, and the four random suppressors

617 (blue).

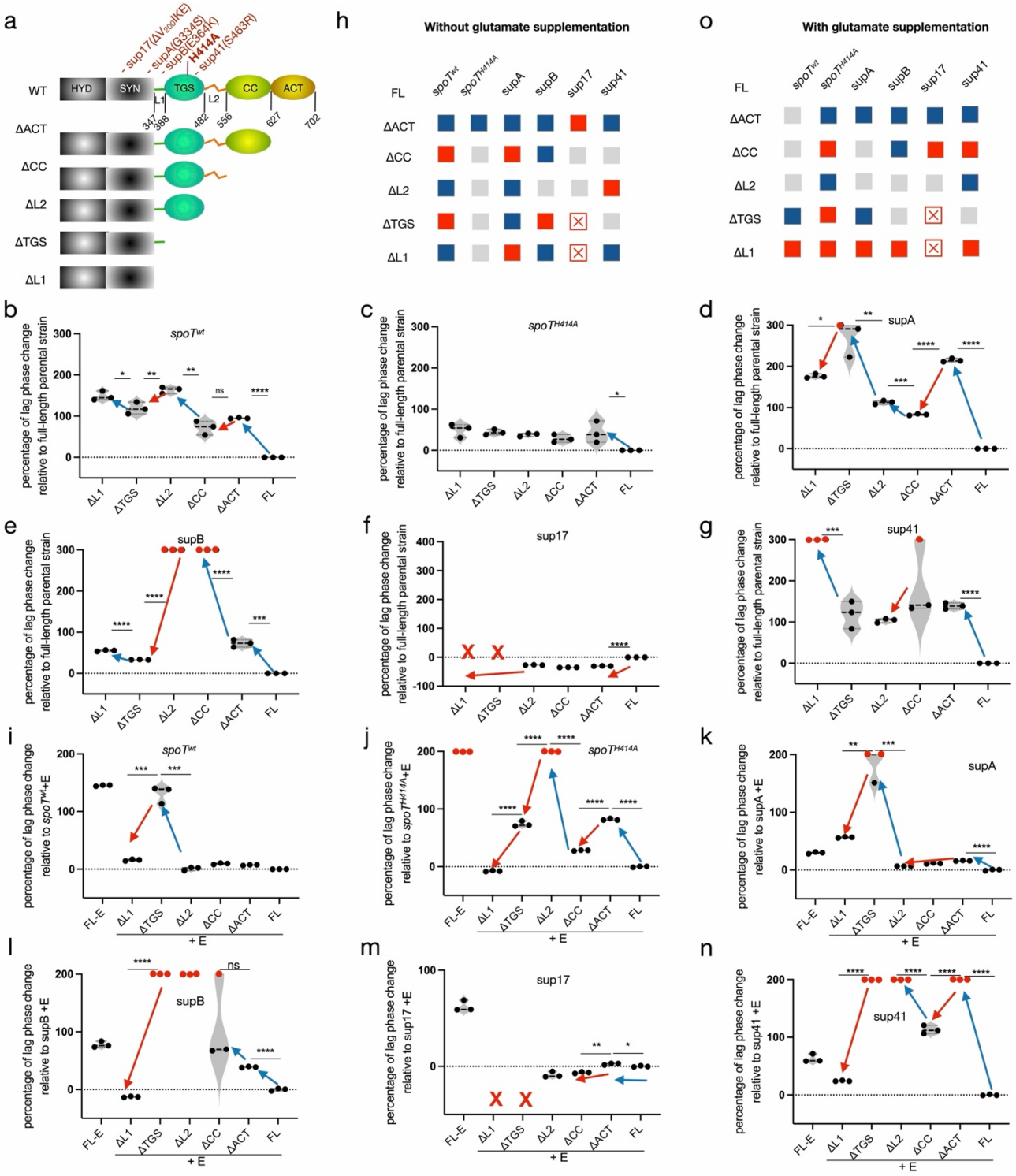

618

619 **Extended Data Fig. 8 Distributed C-terminal domain regulation tunes SpoT-dependent**

620 **growth under basal conditions. (a)** Schematic representation of sequential truncations of SpoT C-

621 terminal regulatory domains introduced into different genetic backgrounds. **(b-g)** Normalized lag

622 phase duration during growth in M9Glc minimal medium, expressed as a percentage relative to the
623 corresponding full-length (FL) SpoT parental strain. Red dots indicate strains that failed to resume
624 growth within the 72-h observation period. Red crosses indicate truncation variants that could not
625 be obtained. **(h)** Summary of the effects of individual domain deletions on growth resumption in
626 M9Glc, based on data in panels **b-g**. Blue and red blocks indicate positive or negative effects on
627 growth, respectively. Red crosses denote non-viable genotypes, and grey blocks indicate conditions
628 in which no clear effect could be inferred due to indistinguishable growth behavior. **(i-n)**
629 Normalized lag phase duration during growth in M9Glc supplemented with glutamate (0.6 mM),
630 expressed relative to the corresponding FL parental strains. **(o)** Summary of domain-specific effects
631 on growth resumption in the presence of glutamate, based on panels **i-n**. Color coding is as in panel
632 **h**.

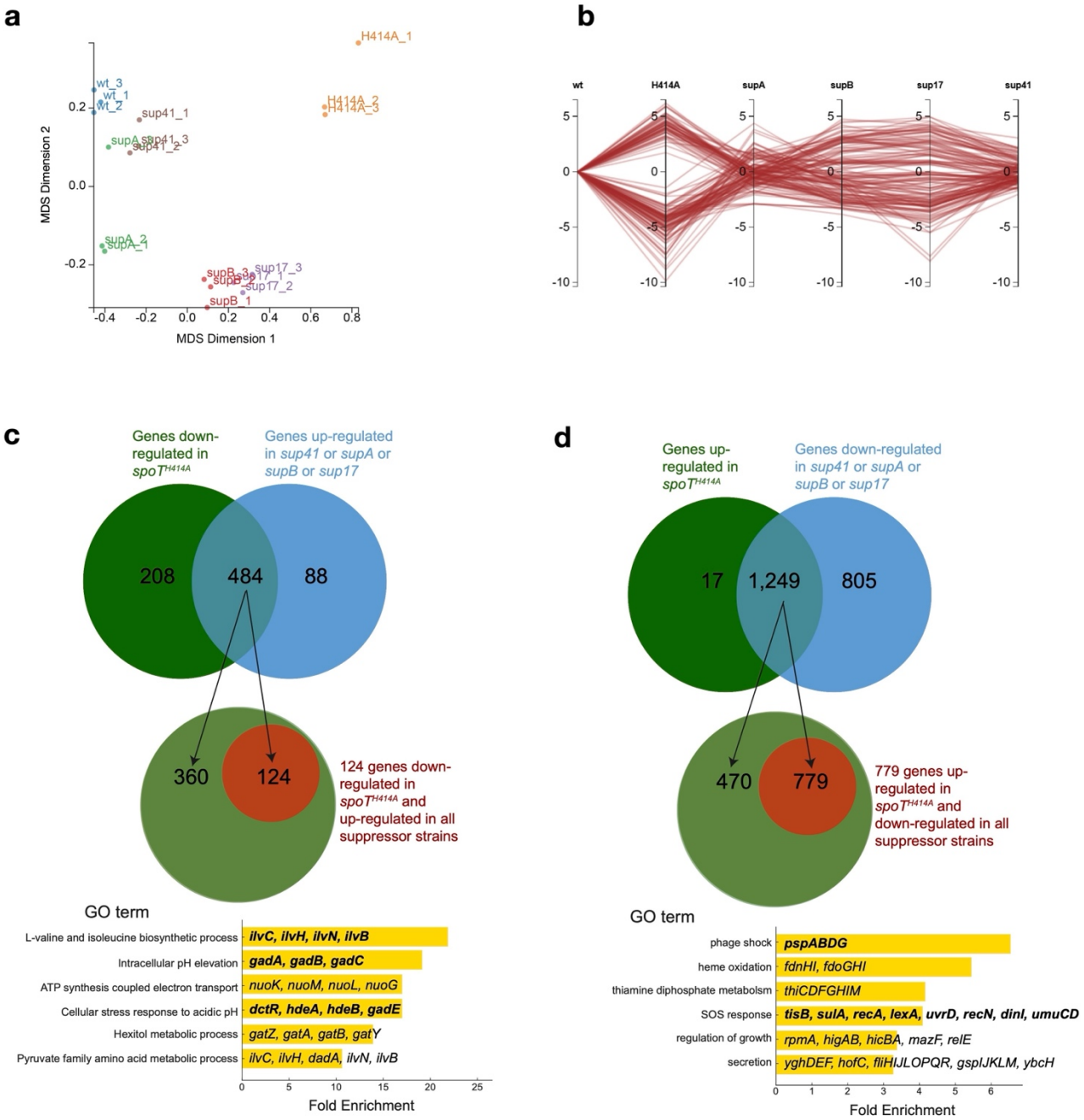

633

634 **Extended Data Fig. 9 Suppressor mutations partially restore global transcriptional programs**

635 **disrupted in *spoT*^{H414A} cells.**

636 **(a)** Parallel coordinates plot showing genes with strong differential expression (|$\log_2$ fold change| >

637 4, FDR < 0.05) across *spoT*^{wt}, *spoT*^{H414A} and four intragenic suppressor strains. (**b**)

638 Multidimensional scaling (MDS) plot of transcriptomic profiles from the same six strains, with

639 individual biological replicates shown. Growth conditions and sampling strategy are described in
640 the Materials and Methods. Panels **a** and **b** were both generated by DEGUST. **(c)** Cross-suppressor
641 analysis of genes downregulated in *spotT*^{H414A}. Top, Venn diagram showing overlap of genes
642 downregulated in *spotT*^{H414A} and upregulated in one or more suppressor strains. Middle, subset of
643 genes downregulated in *spotT*^{H414A} and consistently upregulated in all four suppressor strains.
644 Bottom, Gene Ontology (GO) enrichment analysis of the 124 genes restored across all suppressors.
645 All genes are listed in **Table S4. (d)** Cross-suppressor analysis of genes upregulated in *spotT*^{H414A}.
646 Top, Venn diagram showing overlap of genes upregulated in *spotT*^{H414A} and downregulated in one
647 or more suppressor strains. Middle, subset of genes upregulated in *spotT*^{H414A} and consistently
648 downregulated in all four suppressor strains. Bottom, GO enrichment analysis of the 779 genes
649 consistently repressed across all suppressors. Genes were extracted from DEGUST using thresholds
650 of $|\log_2 \text{fold change}| > 1$ and FDR < 0.05. Gene lists are provided in **Table S4.** Within GO term
651 annotations, gene names shown in bold indicate transcripts with particularly strong differential
652 expression.

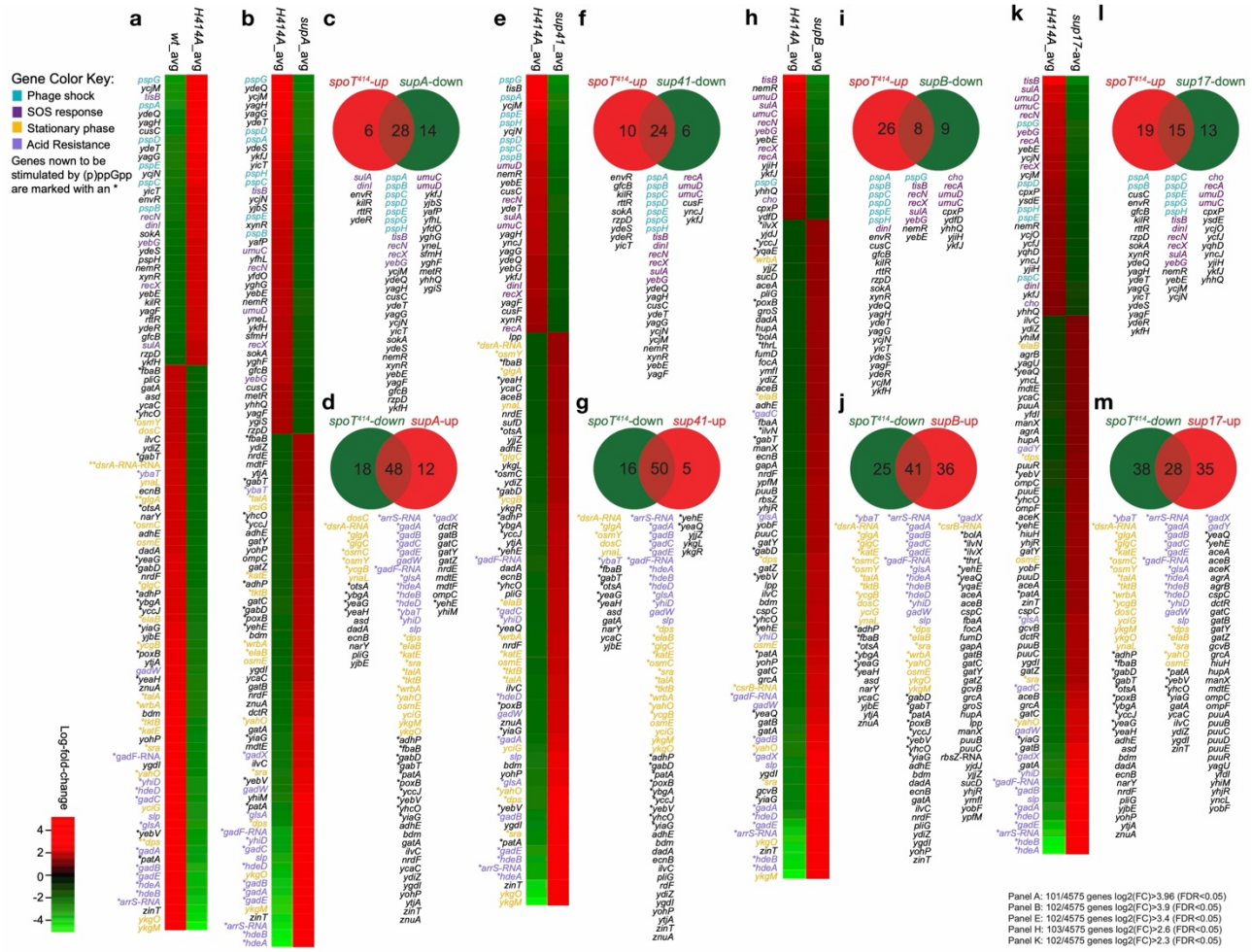

Extended Data Fig. 10 Suppressor mutations differentially correct transcriptional dysregulation in *spoT*^{H414A} cells.

(a) Heatmap of genes differentially expressed in *spoT*^{H414A} relative to *spoT*^{wt}. DEGUST analysis using thresholds of |log$_2$ fold change| > 3.96 and FDR < 0.05 identified 100 genes from a total of 4,575 genes analyzed. Highlighted gene classes include phage shock response genes (*psp*, blue), SOS response genes (magenta), acid stress response genes (deep purple), and stationary-phase-induced genes (gold). Genes marked with an asterisk (*) denote transcripts previously reported to be ppGpp-inducible. (**b, e, h, k)** Heatmaps comparing *spoT*^{H414A} with each suppressor strain. FDR thresholds were identical to those used in panel (**a**), while |log$_2$ fold change| cutoffs were adjusted to return approximately 100 genes per comparison. DEGUST identified 102 genes for supA (|log$_2$ fold

664 change| > 3.9), 97 genes for sup41 (|$\log_2$ fold change| > 3.4), 94 genes for supB (|$\log_2$ fold change| >

665 2.6), and 91 genes for sup17 (|$\log_2$ fold change| > 2.3). Gene lists for each comparison are provided

666 in **Table S5**. **(c, d, f, g, i, j, l, m)** Venn diagram analyses showing overlap of genes dysregulated in

667 *spoT*^{H414A} and in each suppressor strain. Genes differentially expressed in *spoT*^{H414A} relative to

668 *spoT*^{wt} (from panel **a**) were used as the reference gene set for all Venn analyses, with upregulated

669 and downregulated genes analyzed separately.

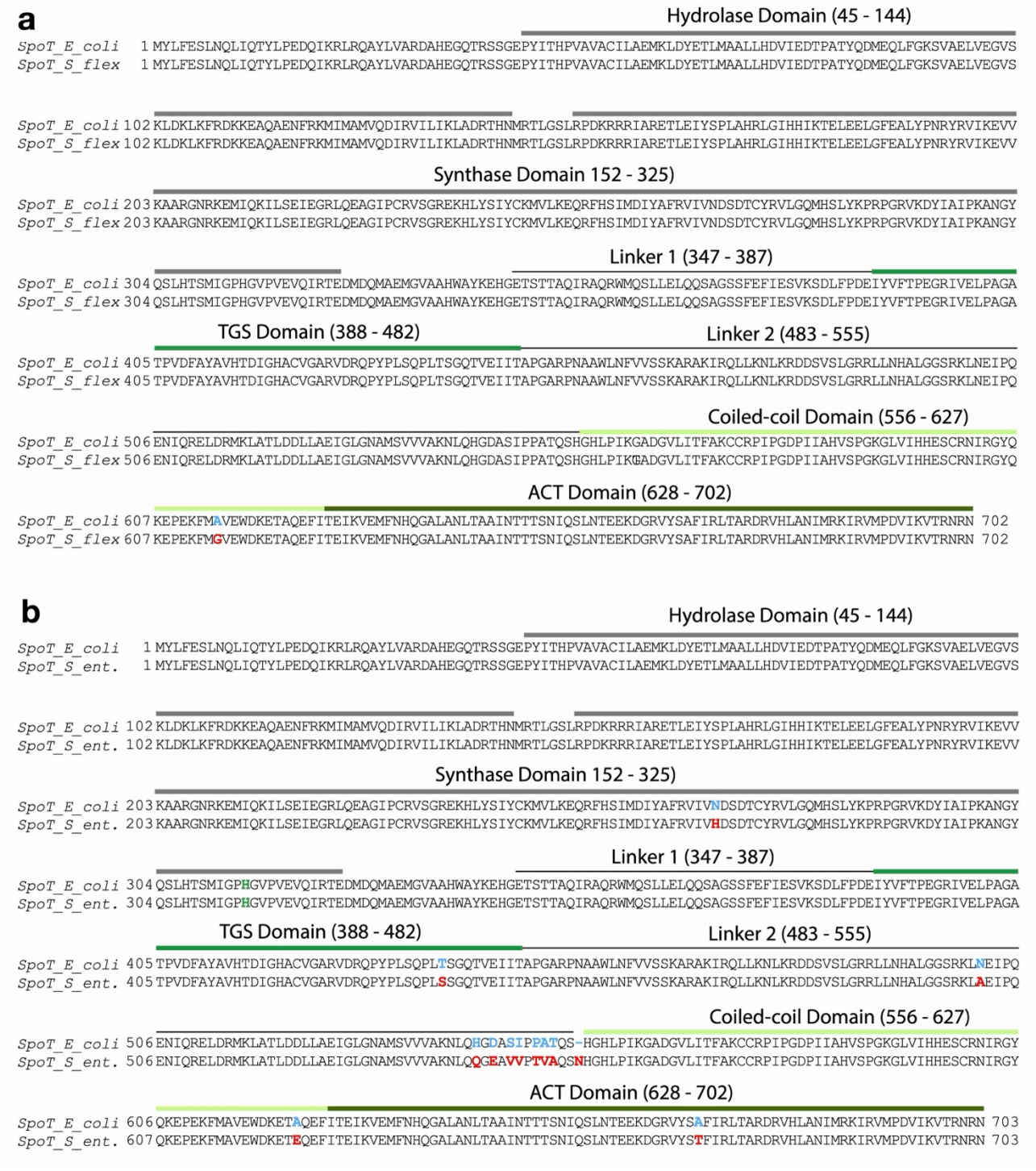

Extended Data Fig. 11 Sequence conservation and divergence of SpoT in enteric bacteria. Pairwise sequence comparison of *Escherichia coli* $SpoT_{ec}$ with SpoT homologs from *Salmonella enterica* serovar Typhimurium SL1334 ($SpoT_{st}$) and *Shigella flexneri* ($SpoT_{sf}$). $SpoT_{sf}$ is nearly identical to $SpoT_{ec}$, differing by a single conserved substitution (A614G) within the CC domain.

675 $SpoT_{st}$ (702 amino acids) shares 98.15% overall sequence identity with $SpoT_{ec}$ (701 amino acids),
676 but contains several amino acid substitutions distributed across multiple domains, including the
677 hydrolase (HYD; N267H), TGS (T437S), linker-2 (L2; nine substitutions: N501A, H542Q, D544E,
678 S546V, I547V, P549T, A550V, T551A, and an insertion of N between residues 553-554), CC
679 (A621E), and ACT (A668T) domains.
680

681 **ACKNOWLEDGEMENTS**

682 We thank Paulina Grucella for helping with Western blot. The work is supported by a Novo Nordisk
683 Foundation Project Grant (NNF19OC0058331), a Danmarks Frie Forskningsfond grant (2032-
684 00030B) to Y.E.Z, the European Union's Horizon 2020 research and innovation programme under
685 the Marie Skłodowska-Curie grant agreement (Nº 801199) to M.L.S, and the Chinese Scholarship
686 Council program (Nº 202206870009) to Y.Y.L.

687

688 **AUTHOR CONTRIBUTIONS**

689 Y.E.Z designed this study; Y.Y.L, M.L.S and Y.E.Z acquired fundings; Y.Y.L, M.L.S, Y.E.Z
690 acquired experimental data; X.C.Z, L.D, K.G, Y.E.Z performed the bioinformatics analyses; Y.E.Z,
691 K.G, wrote the draft manuscript; and all authors analysed the data and edited the manuscript.

692

693 **DECLARATIONS OF INTERESTS**

694 The authors declare that they have no conflicts of interest.

695

696 **EXPERIMENTAL MODEL AND SUBJECT DETAILS**

697 *E. coli* DH5α (Stratagene) was used for cloning and *E. coli* K-12 MG1655 for experiments requiring
698 an *E. coli* wt strain background (see **Table S1** for further details). For cloning, nutrient broth (Oxoid),
699 with agar and antibiotics (chloramphenicol (25 µg/ml), ampicillin (100 µg/ml), and/or kanamycin (25
700 µg/ml)) when appropriate, was used. The different MG1655 strains were cultivated in Lysogeny
701 Broth (LB) as well as M9Glc media (1x M9 salt, pH 7.4 1 mM MgSO4, 0.1 mM $CaCl_2$, Thiamine
702 (0.001 mg/1 ml), 0.2 % (g/ml) glucose) at 37 °C with agitation (160 rpm).

703 **METHOD DETAILS**

704 **Isolation of suppressor mutations rescuing the growth of *spoT*^{H414A} in M9Glc**

705 The *spoT*^{H414A} (YZ527) strain was grown overnight in LB media and then washed twice with PBS
706 buffer. Approx. 10^7 cells were plated on one M9Glc plate and incubated at 30°C. Colonies of different
707 sizes were selected between 24-72 hours of incubation, and the restored growth was confirmed in
708 solid and liquid M9Glc medium.
709
710 **Growth assay in liquid minimal media**
711 To measure the growth curves of various strains in M9Glc media, the OD_{600nm} was measured of
712 overnight cultures grown in LB of each strain, washed twice with 1x Phosphate Buffered Saline (PBS)
713 and normalised in PBS and inoculated into fresh M9Glc media with a starting OD_{600nm} = 0.05 unless
714 otherwise stated. The growth was measured every 15 min for 72 hrs in a plate reader (BioTek)
715 presetted at 30°C with double orbital agitation at 548 cpm. For strains carrying ASKA plasmids (*acpP,*
716 *rsd, ytfK,* or *obgE*), protein expression was induced by addition of IPTG at final concentrations of 20,
717 50, or 200 μM, as indicated.
718
719 **Anti-serum against SpoT C-terminal domains**
720 Because full-length SpoT proved difficult to obtain in a soluble form, we instead generated a
721 truncated SpoT construct encompassing the C-terminal regulatory domains. A DNA fragment
722 corresponding to the *spoT* gene was first amplified using primers pYZ12 and pYZ13 and cloned into
723 the NcoI and BamHI restriction sites of the pET28b expression vector. Subsequently, primers
724 pYZ341 and pYZ342 were used for quick-change mutagenesis to delete the N-terminal catalytic
725 domains, yielding a construct encoding the TGS, CC, and ACT domains of SpoT fused to an N-
726 terminal His_6-TEV tag (pET28b-his.tev.spoT(TGS-CC-ACT)). The resulting plasmid was
727 transformed into *Escherichia coli* BL21(DE3) cells for protein expression. His_6-TEV-SpoT(TGS-
728 CC-ACT) was purified under denaturing conditions using nickel-affinity chromatography. Cell

729 pellets were resuspended in lysis buffer containing 6 M urea (pH 8.0), and clarified lysates were
730 applied to Ni-NTA resin. Bound protein was eluted with buffer containing 50 mM Tris-HCl (pH 8.0),
731 150 mM NaCl, 5% (v/v) glycerol, 0.5 M imidazole, and 6 M urea. Purified His_6-TEV-SpoT(TGS-
732 CC-ACT) protein was used as antigen to generate polyclonal antiserum in rabbits by Covalab
733 (France), according to standard immunization protocols.
734
735 **Unnatural amino acid-mediated UV crosslinking**
736 *Principle of unnatural amino acid-mediated UV crosslinking*
737 Site-specific incorporation of a photo-crosslinkable unnatural amino acid was used to identify
738 potential protein interaction partners of SpoT. A diazirine-containing lysine analog (DiZPK) was
739 incorporated at position H414 of SpoT via amber stop codon suppression, enabling UV-induced
740 covalent crosslinking to proximal proteins under native growth conditions.
741 *Plasmid construction*
742 To generate an amber codon substitution at position H414 of SpoT, the *spoT* gene was amplified from
743 *Escherichia coli* MG1655 genomic DNA using primer pairs pYZ347/348 and pYZ349/350. Overlap
744 PCR was performed to replace the codon encoding H414 with a TAG stop codon. The resulting PCR
745 product was digested with BamHI and EcoRI and cloned into the corresponding sites of the
746 pNDM220 expression vector, generating pNDM220-RBS-His_6.spoT(H414TAG).His_6. To remove
747 the native N-terminal histidine tag sequence, primers pYZ700 and pYZ701 were used to amplify the
748 N-terminal region of *spoT* from MG1655 genomic DNA. This fragment was digested with BamHI
749 and PmlI and cloned into the BamHI/PmlI sites of the intermediate pNDM220-RBS-
750 His_6.spoT(H414TAG).His_6 plasmid, yielding the final construct pNDM220-RBS-
751 spoT(H414TAG).His_6.
752 *Cell growth and unnatural amino acid incorporation*

753 The *E. coli ΔrelA ΔspoT* strain harboring pNDM220-RBS-spoT(H414TAG).His_6 and pSupAR-
754 MbPylRS(DiZPK) (YZ1350) was grown overnight in LB medium and subcultured 1:50 into fresh
755 LB supplemented with 1% (w/v) glucose. Cultures were grown at 30 °C with shaking until OD_{600nm}
756 ≈ 0.2, at which point DiZPK (MedChemExpress; CAS 1337883-32-5) was added to a final
757 concentration of 100 μM. Cells were incubated for an additional 30 min with shaking at 160 rpm,
758 followed by induction of SpoT expression with 1 mM IPTG for 1 h. Cells were then harvested by
759 centrifugation, washed twice with phosphate-buffered saline (PBS), and resuspended in M9Glc
760 medium. Cultures were incubated for an additional 30 min to allow recovery under minimal medium
761 conditions prior to UV crosslinking.

762 *UV crosslinking*

763 Cell density was measured, and an aliquot (1 ml) was collected prior to UV exposure as a non-
764 crosslinked control. Samples were pelleted by centrifugation (13,000 rpm, 2 min), supernatants were
765 removed, and cell pellets were flash-frozen. For crosslinking, cultures were exposed to UV light at
766 365 nm for 30 min using an F8T5BL UV lamp. Following irradiation, cells were harvested by
767 centrifugation, washed once with PBS, pelleted, and stored at −20 °C until analysis.

768 *Protein extraction and immunoblotting*

769 Cell pellets were resuspended in Laemmli sample buffer and normalized to equivalent OD_{600nm}
770 values. Proteins were separated by SDS-PAGE using a 5% resolving gel and transferred to PVDF
771 membranes. Membranes were probed with anti-SpoT antiserum (1:2,000 dilution) for 1 h at room
772 temperature, followed by incubation with HRP-conjugated anti-rabbit secondary antibodies.
773 Immunoreactive bands were detected by chemiluminescence using Pierce® ECL Western Blotting
774 Substrate (Thermo Scientific, #32209) and imaged with an ImageQuant LAS4000 system.

775

776 **Measurements of (p)ppGpp by autoradiography**

777 (p)ppGpp is a highly labile molecule not amenable to HPLC or mass spectrometry analysis. Therefore,
778 thin layer chromatography (TLC) was used to quantify both pppGpp and ppGpp. The excess
779 phosphates in M9Glc affect efficient labelling of nucleotides by $H_3{}^{32}PO_4$, therefore MOPS-M9Glc
780 hybrid media was prepared wherein the PBS buffer in M9Glc was replaced by the MOPS buffer of
781 the MOPS media[44] (i.e., containing MOPS-tricine 40 mM pH 7.2, 1 mM MgSO4, 0.1 mM CaCl2,
782 Thiamine (0.001 mg/1 ml), 0.2 % (g/ml) glucose, NH_4Cl 0.001 g/ml, 8.5 mM NaCl, 0.2 mM $KHPO_4$).
783 The strains were grown for ca. 18 hrs in MOPS-M9Glc media at 37 °C with agitation. Afterwards,
784 the strains were adjusted to the OD_{600nm} of 0.05 in MOPS-M9Glc and grown at 37 °C with agitation
785 until OD_{600nm} of 0.2-0.3 was reached. Then, 100 µl cells were transferred to a 2-ml Eppendorf tube
786 together with 5 µl of 0.005 mCi $H_3{}^{32}PO_4$ (100 µCi/ml, PerkinElmer). After 1h at 37 °C with 600 rpm
787 agitation, 90 µl were transferred to a new tube with 20 µl 2N formic acid, and the sample was stored
788 at -20°C until analysed by TLC as described in[18].
789
790 **Sample preparation for RNA-sequencing**
791 The strains were grown overnight in LB media before washed twice in PBS and inoculated into
792 M9Glc media (OD_{600nm} = 0.05). The strains were grown in M9Glc media until the early exponential
793 phase (approximately OD_{600nm} = 0.2) before the cells were collected, and snap frozen with liquid
794 nitrogen and stored at -80 °C. As the strain *spoT*^{H414A} is unable to grow in M9Glc media, the starting
795 OD_{600nm} was set to 0.2, and the cells were collected when the other strains are ready to harvest, i.e.
796 ca. 18 hrs.
797 Total RNA was extracted using the RNeasy Mini Kit (Qiagen; 74104). Ribosomal RNA (rRNA) was
798 depleted from purified total RNA with Ribo-Zero Plus rRNA Depletion kit (Illumina; 20040892).
799 First and second strand complementary DNA (cDNA) were synthesized by cDNA Synthesis kit
800 (Illumina; 20040895). RNA Index Anchors (Illumina; 20040899) was used for ligation of pre-index

801 anchors to the ends of the double-stranded cDNA fragments to enable dual indexing. Barcoded cDNA
802 libraries were constructed from anchor-ligated DNA fragments and sequenced on Illumina NovaSeq
803 6000 Sequencing System from Genewiz (Azenta Life Sciences), yielding a median depth of
804 39,619,482 paired-end 150 bp reads per sample.
805
806 **Strain construction**
807 All strains and oligonucleotides used in this study are listed in **Tables S1** and **S2**, respectively. All
808 chromosomal *in situ* mutations of *spoT* alleles were made by using the I-SceI-based λ -Red
809 recombineering method[45].
810
811 The *spoT* E319Q and H72A D73A mutant strains
812 Briefly, the pWRG99 plasmid was transformed into the target strains (YZ38, YZ359, YZ543, YZ544,
813 YZ545, YZ546) creating the target strains YZ313, YZ345, YZ826, YZ827, YZ828, and YZ829. The
814 SceI site of the pWRG100 vector was PCR amplified using the primers pYZ611 and pYZ612 for the
815 E319Q mutation and the primers pYZ617 and pYZ618 for the H72A D73A mutation. These PCR
816 DNAs were then electroporated into the above strains (YZ38, YZ359, YZ543, YZ544, YZ545,
817 YZ546). Then, the oligos pYZ613 and pYZ616 were used to introduce the E319Q and H72A D73A
818 mutations into the specific *spoT* alleles *in situ*, generating the E319Q mutant strains (YZ872, YZ873,
819 YZ874, YZ875, YZ876) and H72A D73A mutant strains (YZ900, YZ902, YZ904, YZ905).
820
821 The C-terminal serial truncated mutant strains of *spoT*
822 pYZ796 and pYZ797 were used to amplify the SceI from pWRG100 and introduced into YZ313,
823 YZ345, YZ826, YZ827, YZ828, and YZ829. The serial truncations were performed using the
824 repairing oligos pYZ798, pYZ799, pYZ901, pYZ801, pYZ902, deleting the according domains

825 (ACT, ACT-CC, ACT-CC-Linker2, ACT-CC-Linker2-TGS, ACT-CC-Linker2-TGS-Linker1,
826 respectively).
827
828 Reconstruction of the *spoT*^{H414A} suppressor mutations
829 Primers pYZ619 and pYZ620 were used to amplify the SceI DNA from pWRG100 vector before it
830 was introduced into the strain *spoT*^{wt} (YZ313). Then, the primers pYZ328 and pYZ70 were used to
831 amplify the corresponding *spoT* alleles using the chromosomal DNA of the strains supA (YZ543),
832 *supB* (YZ544), sup17 (YZ545), and sup41 (YZ546) respectively as the templates. These DNAs were
833 used to introduce the specific *spoT* suppressing mutations.
834
835 P1 phage transduction
836 The *spoT* genes of the suppressor strains YZ543, YZ544, YZ545, and YZ546 were inactivated via
837 P1 phage transduction. The donor strain for making the P1 phage lysate was the *spoT207::cat* strain
838 (YZ47)[13], which contains a chloramphenicol resistance cassette together with *spoT207* deletion allele
839 for selection. The phage lysate was used to infect strains YZ543, YZ544, YZ545, and YZ546 and the
840 chloramphenicol resistant transductants were selected and confirmed via diagnostic PCR.
841
842 **Plasmids constructions**
843 To construct *E. coli (Ec), Salmonella typhimurium(st) or Shigella flexneri(sf) spoT* wild type (wt) and
844 H414A mutant plasmids, standard molecular cloning procedures were used. For *E. coli*, the *spoT*
845 coding sequence was PCR-amplified from MG1655 *spoT*^{wt} (YZ38) or *spoT*^{H414A} (YZ527) using
846 primers pYZ1201 and pYZ1202. The pBAD33 vector was isolated from *E. coli* DH5α (YZ593). Both
847 the amplified *spoT* fragments and pBAD33 were digested with *KpnI* and *HindIII* and ligated using
848 T4 DNA ligase to generate pBAD33- *spoT*^{wt} and pBAD33- *spoT*^{H414A}. For *S. Typhimurium*, the

849 H414A mutation was introduced into pGEN-MCS-*spoT*$_{St}$ (YZ692)[46] by site-directed mutagenesis
850 using primers pYZ1312 and pYZ1313, yielding pGEN-MCS-spoT$_{st}$ (H414A). For *S. flexneri*, an
851 A614G substitution was introduced by overlap-extension PCR using pBAD33-*spoT*$_{Ec}$(wt) or
852 pBAD33- *spoT*$_{Ec}$(H414A) as templates. Upstream and downstream fragments were amplified with
853 primer pairs pYZ1201/pYZ1346 and pYZ1202/pYZ1345, respectively, fused by overlap PCR using
854 primers pYZ1201 and pYZ1202, and cloned into pBAD33 following digestion with *KpnI* and *HindIII*
855 to generate pBAD33-*spoT*$_{Sf}$(WT) and pBAD33-*spoT*$_{Sf}$(H414A). To construct the plasmid pCA24N-
856 argA(H15Y), quick-change mutagenesis was carried out using pCA24N-argA(wt) as template and
857 the primers pYZ1168 and pYZ1169. All plasmids were transformed into *E. coli* DH5α (see **Table**
858 **S1**), purified using a commercial miniprep kit (NEB-T1110L), and confirmed by sequencing with
859 primers pYZ404, pYZ405, and pYZ71 (for pBAD33 constructs), pYZ1305, pYZ1306, and pYZ1228
860 (for pGEN-MCS constructs) or pYZ34 and pYZ35 (for pCA24N constructs; Eurofins Genomics).

861

862 **Acid resistance assay**

863 Overnight (16 hrs) cultures were grown in LB medium at 37°C with shaking (160 rpm). Cells were
864 harvested by centrifugation, washed twice with PBS, and normalized to an optical density at 600 nm
865 (OD_{600nm}) of 0.4 in minimal medium supplemented with 0.2% glucose (M9Glc, pH 7.4). Cultures
866 were incubated at 37°C with shaking (160 rpm) for 30 min to allow adaptation to M9Glc. After
867 adaptation, 1 mL cells were pelleted and resuspended in the same volume of M9Glc medium pre-
868 adjusted to various pH values (from 2.5 to 8.0), with or without supplemented 0.6 mM glutamate (or
869 other amino acids). Acid challenge was then performed and assessed at 37°C with shaking (160 rpm).
870 Cell viability was determined at time zero (i.e., before shifting to M9Glc with a low pH), and at 0.5,
871 1, 2 and 4 h after acid challenges. For viable-cell counts, 40 μL cell culture at each time point was

872 collected and 10-fold serially diluted (10^0-10^{-7}) in LB medium, and 5 µL of each dilution was spotted
873 on LB agar plates, allowing colony formation and enumeration and calculation of CFUs the next day.
874
875 **Western blot**
876 Western blot analysis of protein levels of various mutant SpoT was performed as reported[18]. Briefly,
877 cells of various strains were collected the same manner as preparation for RNA sequencing (see above,
878 and **Fig. S1C**). These cells were normalised to have an equal OD_{600nm} per ml and mixed with 2x SDS-
879 PAGE loading buffer. Samples were heated for 15 min at 95°C and 20 ul of each were separated in
880 10% SDS-PAGE gels. The proteins were transferred to a PVDF membrane (Amersham) and the SpoT
881 proteins detected by first incubation with anti-SpoT antiserum (Covalab) and then the secondary HRP
882 conjugated rabbit IgG antibody (SIGMA). The SpoT bands were visualized by using the Pierce ECL
883 chemiluminescence substrate (Thermo) and the signals were detected by an Imagequant LAS4100.
884
885 **Bioinformatic analysis**
886 Preparing RNA-seq data. RNA-seq data (fastq files) were mapped by the BWA-MEM tool of
887 Galaxy[47] and then analysed by the featureCounts tool in Galaxy https://usegalaxy.eu/). The tabular
888 format of the featureCounts files were exported from Galaxy and assembled into one single tabular
889 file from which sub-files containing collections of genes of interest, e.g. amino acid biosynthesis,
890 purine de novo synthesis, were extracted.
891
892 Analysis of RNA-seq data. To generate heatmaps and fold-of-changes, the tabular files containing
893 the RNA-seq counts were analysed by DEGUST (https://degust.erc.monash.edu/). To generate
894 Venn diagrams, gene lists were analysed by the jVenn application at
895 (https://jvenn.toulouse.inrae.fr/app/index.html). Gene Ontology terms were generated by AmiGO

896 (https://amigo.geneontology.org/amigo) and Panther

897 (https://pantherdb.org/webservices/go/overrep.jsp). The json-files generated by PANTHER were

898 analysed by ChatGPT that generated editable SVG files.

899

900 Other Bioinformatic Procedures

901 Protein sequence alignment was accomplished using JalView[48], protein tertiary structure modelling

902 and visualization by AlphaFold 3 and ChimeraX, respectively[49,50].

903

904 **QUANTIFICATION AND STATISTICAL ANALYSIS**

905 Signals of (p)ppGpp from autoradiography were quantified using ImageQuant (GE Healthcare). At

906 least three biological replicates were performed and one representative shown in the **Figure**s.

907 For other physiological growth experiments, at least two biological replicates each with three

908 technical replicates were done (see **Figure** legends for details). The length (hours) of lag phases was

909 defined as the period from the growth start to the time point where the slope of growth curves first

910 reaches the exponential-phase growth rate. These lag phage length values were then normalized to

911 the parental strains or conditions, and plotted (see each of the legends for details). The student *t*-test

912 was used for statistic analysis wherever applicable.

913

914 **DATA AVAILABILITY**

915 The RNA-seq raw data produced in this study are available through the NCBI Sequence Read

916 Archive under BioProject accession number PRJNA1097790.

References

1. Fang, F.C., Frawley, E.R., Tapscott, T., and Vázquez-Torres, A. (2016). Bacterial Stress Responses during Host Infection. Cell Host Microbe *20*, 133-143. 10.1016/j.chom.2016.07.009.
2. Kanjee, U., and Houry, W.A. (2013). Mechanisms of acid resistance in Escherichia coli. Annu Rev Microbiol *67*, 65-81. 10.1146/annurev-micro-092412-155708.
3. Irving, S.E., Choudhury, N.R., and Corrigan, R.M. (2021). The stringent response and physiological roles of (pp)pGpp in bacteria. Nat Rev Microbiol *19*, 256-271. 10.1038/s41579-020-00470-y.
4. Anderson, B.W., Fung, D.K., and Wang, J.D. (2021). Regulatory Themes and Variations by the Stress-Signaling Nucleotide Alarmones (p)ppGpp in Bacteria. Annu Rev Genet *55*, 115-133. 10.1146/annurev-genet-021821-025827.
5. Bange, G., Brodersen, D.E., Liuzzi, A., and Steinchen, W. (2021). Two P or Not Two P: Understanding Regulation by the Bacterial Second Messengers (p)ppGpp. Annu Rev Microbiol *75*, 383-406. 10.1146/annurev-micro-042621-122343.
6. Hauryliuk, V., Atkinson, G.C., Murakami, K.S., Tenson, T., and Gerdes, K. (2015). Recent functional insights into the role of (p)ppGpp in bacterial physiology. Nat Rev Microbiol *13*, 298-309. 10.1038/nrmicro3448.
7. Block, R., and Haseltine, A.W. (1975). Purification and properties of stringent factor. J Biol Chem *250*, 1212-1217.
8. Brown, A., Fernandez, I.S., Gordiyenko, Y., and Ramakrishnan, V. (2016). Ribosome-dependent activation of stringent control. Nature *534*, 277-280. 10.1038/nature17675.
9. Loveland, A.B., Bah, E., Madireddy, R., Zhang, Y., Brilot, A.F., Grigorieff, N., and Korostelev, A.A. (2016). Ribosome•RelA structures reveal the mechanism of stringent response activation. Elife *5*. 10.7554/eLife.17029.
10. Arenz, S., Abdelshahid, M., Sohmen, D., Payoe, R., Starosta, A.L., Berninghausen, O., Hauryliuk, V., Beckmann, R., and Wilson, D.N. (2016). The stringent factor RelA adopts an open conformation on the ribosome to stimulate ppGpp synthesis. Nucleic Acids Res *44*, 6471-6481. 10.1093/nar/gkw470.
11. Winther, K.S., Roghanian, M., and Gerdes, K. (2018). Activation of the Stringent Response by Loading of RelA-tRNA Complexes at the Ribosomal A-Site. Mol Cell *70*, 95-105.e104. 10.1016/j.molcel.2018.02.033.
12. Ross, W., Vrentas, C.E., Sanchez-Vazquez, P., Gaal, T., and Gourse, R.L. (2013). The magic spot: a ppGpp binding site on E. coli RNA polymerase responsible for regulation of transcription initiation. Mol Cell *50*, 420-429. 10.1016/j.molcel.2013.03.021.
13. Ross, W., Sanchez-Vazquez, P., Chen, A.Y., Lee, J.H., Burgos, H.L., and Gourse, R.L. (2016). ppGpp Binding to a Site at the RNAP-DksA Interface Accounts for Its Dramatic Effects on Transcription Initiation during the Stringent Response. Mol Cell *62*, 811-823. 10.1016/j.molcel.2016.04.029.
14. Durfee, T., Hansen, A.M., Zhi, H., Blattner, F.R., and Jin, D.J. (2008). Transcription profiling of the stringent response in Escherichia coli. J Bacteriol *190*, 1084-1096. 10.1128/jb.01092-07.
15. Traxler, M.F., Summers, S.M., Nguyen, H.T., Zacharia, V.M., Hightower, G.A., Smith, J.T., and Conway, T. (2008). The global, ppGpp-mediated stringent response to amino acid

starvation in Escherichia coli. Mol Microbiol *68*, 1128-1148. 10.1111/j.1365-2958.2008.06229.x.

16. Sanchez-Vazquez, P., Dewey, C.N., Kitten, N., Ross, W., and Gourse, R.L. (2019). Genome-wide effects on Escherichia coli transcription from ppGpp binding to its two sites on RNA polymerase. Proc Natl Acad Sci U S A *116*, 8310-8319. 10.1073/pnas.1819682116.
17. Zhang, Y., Zborníková, E., Rejman, D., and Gerdes, K. (2018). Novel (p)ppGpp Binding and Metabolizing Proteins of Escherichia coli. mBio *9*. 10.1128/mBio.02188-17.
18. Zhang, Y.E., Baerentsen, R.L., Fuhrer, T., Sauer, U., Gerdes, K., and Brodersen, D.E. (2019). (p)ppGpp Regulates a Bacterial Nucleosidase by an Allosteric Two-Domain Switch. Mol Cell *74*, 1239-1249 e1234. 10.1016/j.molcel.2019.03.035.
19. Wang, B., Dai, P., Ding, D., Del Rosario, A., Grant, R.A., Pentelute, B.L., and Laub, M.T. (2019). Affinity-based capture and identification of protein effectors of the growth regulator ppGpp. Nat Chem Biol *15*, 141-150. 10.1038/s41589-018-0183-4.
20. Wang, B., Grant, R.A., and Laub, M.T. (2020). ppGpp Coordinates Nucleotide and Amino-Acid Synthesis in E. coli During Starvation. Mol Cell *80*, 29-42.e10. 10.1016/j.molcel.2020.08.005.
21. Grucela, P.K., Fuhrer, T., Sauer, U., Chao, Y., and Zhang, Y.E. (2023). Ribose 5-phosphate: the key metabolite bridging the metabolisms of nucleotides and amino acids during stringent response in Escherichia coli? Microb Cell *10*, 141-144. 10.15698/mic2023.07.799.
22. Fernández-Coll, L., and Cashel, M. (2020). Possible Roles for Basal Levels of (p)ppGpp: Growth Efficiency Vs. Surviving Stress. Front Microbiol *11*, 592718. 10.3389/fmicb.2020.592718.
23. Xiao, H., Kalman, M., Ikehara, K., Zemel, S., Glaser, G., and Cashel, M. (1991). Residual guanosine 3',5'-bispyrophosphate synthetic activity of relA null mutants can be eliminated by spoT null mutations. J Biol Chem *266*, 5980-5990.
24. Seyfzadeh, M., Keener, J., and Nomura, M. (1993). spoT-dependent accumulation of guanosine tetraphosphate in response to fatty acid starvation in Escherichia coli. Proc Natl Acad Sci U S A *90*, 11004-11008.
25. Battesti, A., and Bouveret, E. (2006). Acyl carrier protein/SpoT interaction, the switch linking SpoT-dependent stress response to fatty acid metabolism. Mol Microbiol *62*, 1048-1063. 10.1111/j.1365-2958.2006.05442.x.
26. Vinella, D., Albrecht, C., Cashel, M., and D'Ari, R. (2005). Iron limitation induces SpoT-dependent accumulation of ppGpp in Escherichia coli. Mol Microbiol *56*, 958-970. 10.1111/j.1365-2958.2005.04601.x.
27. Spira, B., Silberstein, N., and Yagil, E. (1995). Guanosine 3',5'-bispyrophosphate (ppGpp) synthesis in cells of Escherichia coli starved for Pi. J Bacteriol *177*, 4053-4058. 10.1128/jb.177.14.4053-4058.1995.
28. Levin-Reisman, I., Ronin, I., Gefen, O., Braniss, I., Shoresh, N., and Balaban, N.Q. (2017). Antibiotic tolerance facilitates the evolution of resistance. Science *355*, 826-830. 10.1126/science.aaj2191.
29. Windels, E.M., Michiels, J.E., Fauvart, M., Wenseleers, T., Van den Bergh, B., and Michiels, J. (2019). Bacterial persistence promotes the evolution of antibiotic resistance by increasing survival and mutation rates. Isme j *13*, 1239-1251. 10.1038/s41396-019-0344-9.
30. Lewis, K. (2007). Persister cells, dormancy and infectious disease. Nat Rev Microbiol *5*, 48-56. 10.1038/nrmicro1557.
31. Dalebroux, Z.D., Svensson, S.L., Gaynor, E.C., and Swanson, M.S. (2010). ppGpp conjures bacterial virulence. Microbiol Mol Biol Rev *74*, 171-199. 10.1128/mmbr.00046-09.

1009 32. Harms, A., Maisonneuve, E., and Gerdes, K. (2016). Mechanisms of bacterial persistence
1010 during stress and antibiotic exposure. Science *354*. 10.1126/science.aaf4268.
1011 33. Lin, J., Smith, M.P., Chapin, K.C., Baik, H.S., Bennett, G.N., and Foster, J.W. (1996).
1012 Mechanisms of acid resistance in enterohemorrhagic Escherichia coli. Appl Environ
1013 Microbiol *62*, 3094-3100. 10.1128/aem.62.9.3094-3100.1996.
1014 34. Lund, P., Tramonti, A., and De Biase, D. (2014). Coping with low pH: molecular strategies
1015 in neutralophilic bacteria. FEMS Microbiol Rev *38*, 1091-1125. 10.1111/1574-6976.12076.
1016 35. Capitani, G., De Biase, D., Aurizi, C., Gut, H., Bossa, F., and Grütter, M.G. (2003). Crystal
1017 structure and functional analysis of Escherichia coli glutamate decarboxylase. Embo j *22*,
1018 4027-4037. 10.1093/emboj/cdg403.
1019 36. Castanie-Cornet, M.P., Penfound, T.A., Smith, D., Elliott, J.F., and Foster, J.W. (1999).
1020 Control of acid resistance in Escherichia coli. J Bacteriol *181*, 3525-3535.
1021 10.1128/jb.181.11.3525-3535.1999.
1022 37. Rajagopal, B.S., DePonte, J., 3rd, Tuchman, M., and Malamy, M.H. (1998). Use of inducible
1023 feedback-resistant N-acetylglutamate synthetase (argA) genes for enhanced arginine
1024 biosynthesis by genetically engineered Escherichia coli K-12 strains. Appl Environ Microbiol
1025 *64*, 1805-1811. 10.1128/aem.64.5.1805-1811.1998.
1026 38. Persky, N.S., Ferullo, D.J., Cooper, D.L., Moore, H.R., and Lovett, S.T. (2009). The
1027 ObgE/CgtA GTPase influences the stringent response to amino acid starvation in Escherichia
1028 coli. Mol Microbiol *73*, 253-266. 10.1111/j.1365-2958.2009.06767.x.
1029 39. Lee, J.W., Park, Y.H., and Seok, Y.J. (2018). Rsd balances (p)ppGpp level by stimulating the
1030 hydrolase activity of SpoT during carbon source downshift in Escherichia coli. Proc Natl Acad
1031 Sci U S A *115*, E6845-E6854. 10.1073/pnas.1722514115.
1032 40. Germain, E., Guiraud, P., Byrne, D., Douzi, B., Djendli, M., and Maisonneuve, E. (2019).
1033 YtfK activates the stringent response by triggering the alarmone synthetase SpoT in
1034 Escherichia coli. Nat Commun *10*, 5763. 10.1038/s41467-019-13764-4.
1035 41. Zhou, Y.N., and Jin, D.J. (1998). The rpoB mutants destabilizing initiation complexes at
1036 stringently controlled promoters behave like "stringent" RNA polymerases in Escherichia coli.
1037 Proc Natl Acad Sci U S A *95*, 2908-2913. 10.1073/pnas.95.6.2908.
1038 42. Kitagawa, M., Ara, T., Arifuzzaman, M., Ioka-Nakamichi, T., Inamoto, E., Toyonaga, H., and
1039 Mori, H. (2005). Complete set of ORF clones of Escherichia coli ASKA library (a complete
1040 set of E. coli K-12 ORF archive): unique resources for biological research. DNA Res *12*, 291-
1041 299. 10.1093/dnares/dsi012.
1042 43. Saka, K., Tadenuma, M., Nakade, S., Tanaka, N., Sugawara, H., Nishikawa, K., Ichiyoshi, N.,
1043 Kitagawa, M., Mori, H., Ogasawara, N., and Nishimura, A. (2005). A complete set of
1044 Escherichia coli open reading frames in mobile plasmids facilitating genetic studies. DNA
1045 Res *12*, 63-68.
1046 44. Neidhardt, F.C., Bloch, P.L., and Smith, D.F. (1974). Culture medium for enterobacteria. J
1047 Bacteriol *119*, 736-747. 10.1128/jb.119.3.736-747.1974.
1048 45. Kanjee, U., Gutsche, I., Alexopoulos, E., Zhao, B., El Bakkouri, M., Thibault, G., Liu, K.,
1049 Ramachandran, S., Snider, J., Pai, E.F., and Houry, W.A. (2011). Linkage between the
1050 bacterial acid stress and stringent responses: the structure of the inducible lysine
1051 decarboxylase. Embo j *30*, 931-944. 10.1038/emboj.2011.5.
1052 46. Chau, N.Y.E., Perez-Morales, D., Elhenawy, W., Bustamante, V.H., Zhang, Y.E., and
1053 Coombes, B.K. (2021). (p)ppGpp-Dependent Regulation of the Nucleotide Hydrolase PpnN
1054 Confers Complement Resistance in Salmonella enterica Serovar Typhimurium. Infect Immun
1055 *89*. 10.1128/IAI.00639-20.

47. The Galaxy platform for accessible, reproducible, and collaborative data analyses: 2024 update. (2024). Nucleic Acids Res *52*, W83-w94. 10.1093/nar/gkae410.
48. Procter, J.B., Carstairs, G.M., Soares, B., Mourão, K., Ofoegbu, T.C., Barton, D., Lui, L., Menard, A., Sherstnev, N., Roldan-Martinez, D., et al. (2021). Alignment of Biological Sequences with Jalview. Methods Mol Biol *2231*, 203-224. 10.1007/978-1-0716-1036-7_13.
49. Senior, A.W., Evans, R., Jumper, J., Kirkpatrick, J., Sifre, L., Green, T., Qin, C., Žídek, A., Nelson, A.W.R., Bridgland, A., et al. (2020). Improved protein structure prediction using potentials from deep learning. Nature *577*, 706-710. 10.1038/s41586-019-1923-7.
50. Pettersen, E.F., Goddard, T.D., Huang, C.C., Meng, E.C., Couch, G.S., Croll, T.I., Morris, J.H., and Ferrin, T.E. (2021). UCSF ChimeraX: Structure visualization for researchers, educators, and developers. Protein Sci *30*, 70-82. 10.1002/pro.3943.

1069 **Legends to Supplementary Tables**

1070 **Table S1. Bacterial strains used in this study**

1071 **Table S2. Oligonucleotides used in this study**

1072 **Table S3. Differential gene expression analysis of RNA-seq data from *spoT*^{wt} and *spoT*^{H414A}**

1073 **strains .** In total, the transcription levels of 4575 genes of MG1655 were analysed. At a setting of

1074 |Log2(FC)| > 1 and FDR < 0.05, 865 and 949 genes were down and up-regulated, respectively. The

1075 change-of-folds |Log2(FC)| of each gene are also shown.

1076

1077 **Table S4. Gene ontology analysis of the four suppressor strains.**

1078 **Sheet #1 (related to Extended Data Fig. 7C):** Genes downregulated in the *spoT*^{H414A} strain relative

1079 to the *spoT*^{wt} strain (Column A). Genes upregulated in either of the four suppressor strains *supA*,

1080 *sup41*, *supB* and *sup17* relative to the *spoT*^{H414A} strain (Columns B to E). The list of genes in

1081 Columns B to E were used to generate a list of genes that were upregulated in at least one

1082 suppressor strain (Column F) and a list of genes that were upregulated in all 4 suppressor strains

1083 (Column G).

1084

1085 **Sheet #2 (related to Extended Data Fig. 7D):** Genes upregulated in the *spoT*^{H414A} strain relative

1086 to the *spoT*^{wt} strain (Column A). Genes downregulated in either of the four suppressor strains

1087 relative to the *spoT*^{H414A} strain. The list of genes in Columns B to E were used to generate a list of

1088 genes that were upregulated in at least one suppressor strain (Column F) and a list of genes that

1089 were downregulated in all 4 suppressor strains (Column G). Gene lists in **Table S4** were generated

1090 by DEGUST at a setting of |Log2(FC)| > 1 and FRD < 0.05.

1091

1092 **Table S5. Comparison of *spoT*^{H414A} with suppressor strains (related to Extended Data Fig. 8).**

1093 The Table yields the folds-of-changes in the suppressor strains relative to *spoT*^{H414A}. The Log2(FC)

1094 setting in DEGUST was chosen to yield around 100 genes up and downregulated in each heatmap

1095 Panels a, b, e, h and k of **Extended Data Fig. 8**.